**Article**
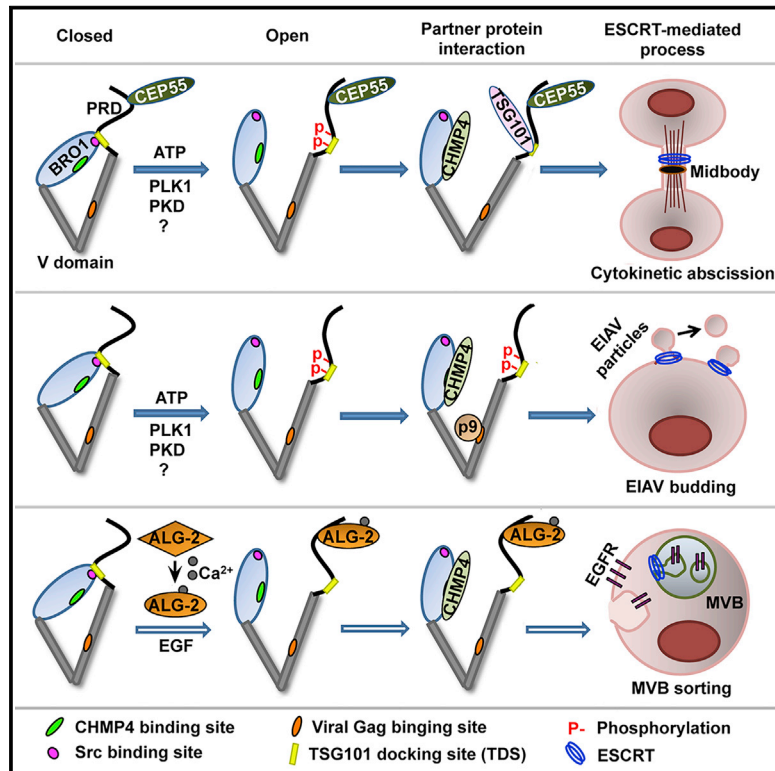
# Phosphorylation-Dependent Activation of the ESCRT Function of ALIX in Cytokinetic Abscission and Retroviral Budding

## Graphical Abstract



## Authors

Sheng Sun, Le Sun, Xi Zhou, Chuanfen Wu, Ruoning Wang, Sue-Hwa Lin, Jian Kuang

## Correspondence

jkuang@mdanderson.org

## In Brief

The widely expressed adaptor protein ALIX promotes membrane scission during cytokinesis, retroviral budding, and endolysosomal trafficking of activated growth factor receptors. Sun et al. identify a phosphorylation-dependent mechanism that relieves ALIX auto-inhibition and specifically activates its membrane-remodeling function in cytokinetic abscission and retroviral budding, but not in receptor trafficking.

## Highlights

- Cytosolic ALIX changes from closed to open conformation during M phase induction

- Phosphorylation of the S718-S721 residues produces an open conformation of ALIX

- S718-S721 phosphorylation allows ALIX to function in cytokinetic abscission

- S718-S721 phosphorylation is required for ALIX to support EIAV budding

CellPress

# Article

# Phosphorylation-Dependent Activation of the ESCRT Function of ALIX in Cytokinetic Abscission and Retroviral Budding

Sheng Sun,[1,2] Le Sun,[3] Xi Zhou,[1] Chuanfen Wu,[1] Ruoning Wang,[1,5] Sue-Hwa Lin,[2,4] and Jian Kuang[1,2,*]

[1]Department of Experimental Therapeutics, The University of Texas MD Anderson Cancer Center, Houston, TX 77230, USA
[2]Experimental Therapeutics Academic Program, The University of Texas Graduate School of Biomedical Sciences at Houston, Houston, TX 77030, USA
[3]AbMax Biotechnology, Beijing 100085, China
[4]Department of Translational Molecular Pathology, The University of Texas MD Anderson Cancer Center, Houston, TX 77030, USA
[5]Present address: Center for Childhood Cancer & Blood Diseases, Hematology/Oncology & BMT, The Research Institute at Nationwide Children's Hospital, Ohio State University, Columbus, OH 43205, USA
*Correspondence: jkuang@mdanderson.org
http://dx.doi.org/10.1016/j.devcel.2016.01.001

## SUMMARY

The modular adaptor protein ALIX is a key player in multiple ESCRT-III-mediated membrane remodeling processes. ALIX is normally present in a closed conformation due to an intramolecular interaction that renders ALIX unable to perform its ESCRT functions. Here we demonstrate that M phase-specific phosphorylation of the intramolecular interaction site within the proline-rich domain (PRD) of ALIX transforms cytosolic ALIX from closed to open conformation. Defining the role of this mechanism of ALIX regulation in three classical ESCRT-mediated processes revealed that phosphorylation of the intramolecular interaction site in the PRD is required for ALIX to function in cytokinetic abscission and retroviral budding, but not in multivesicular body sorting of activated epidermal growth factor receptor. Thus, phosphorylation of the intramolecular interaction site in the PRD is one of the major mechanisms that activates the ESCRT function of ALIX.

## INTRODUCTION

The endosome sorting complexes required for transport (ESCRT) proteins constitute an evolutionary conserved membrane remodeling system that buds membranes and severs membrane necks in the opposite topology of endocytosis (Henne et al., 2011, 2013; Hurley, 2015). The best-characterized functions of ESCRT proteins are the multivesicular body (MVB) sorting of internalized membrane receptors (Babst et al., 2002a, 2002b; Katzmann et al., 2001), the budding of enveloped retroviruses from infected cells (Strack et al., 2003; von Schwedler et al., 2003), and the membrane scission at the end of cytokinesis (Carlton and Martin-Serrano, 2007; Morita et al., 2007). The central event in ESCRT-mediated membrane remodeling is the assembly of a highly oligomerized ESCRT-III

complex from monomeric proteins (McCullough et al., 2015; Teis et al., 2008), followed by the timely disassembly of this complex by the ATPase Vps4 (Caillat et al., 2015; Yang et al., 2015). Upstream of the core event, ALIX (ALG-2 interacting protein X), in parallel with the ESCRT-I-ESCRT-II complex, binds both a membrane remodeling cargo and the ESCRT-III component CHMP4 to initiate ESCRT-III assembly at the right time and in the right location (Carlson and Hurley, 2012; Pashkova et al., 2013).

Structural studies of ALIX revealed that ALIX consists of an N-terminal banana-shaped Bro1 domain, a middle V letter-shaped domain, and an intrinsically disordered C-terminal proline-rich domain (PRD) (Fisher et al., 2007). The Bro1 domain contains a 3D docking site for CHMP4 (hydrophobic Patch 1) and a linear docking site for Src (hydrophobic Patch 2) (Kim et al., 2005; McCullough et al., 2008). The V domain contains a 3D hydrophobic pocket around F676 (the F676 pocket), which is the docking site for retroviral Gag proteins (Lee et al., 2007; Zhai et al., 2008). The PRD contains two linear docking sites (717–720 and 852–855) for the ESCRT-I component TSG101 and an ALIX multimerization sequence (Carlton et al., 2008). Using monoclonal antibodies that recognize different epitopes in ALIX, we discovered that cytosolic ALIX is normally present in a closed conformation that is unable to interact with CHMP4, Src, or viral GAG (Zhou et al., 2008, 2009). This is achieved through an intramolecular interaction between the Src docking site in the Bro1 domain and the first TSG101 docking site (TDS) in the PRD (Zhou et al., 2010). These findings predict that relieving the intramolecular interaction of ALIX is critical for multiple ESCRT-III mediated processes.

In MVB sorting of activated epidermal growth factor receptor (EGFR), calcium-dependent ALG-2 interaction with cytosolic ALIX relieves its intramolecular interaction and promotes its association with the membrane through interaction with membrane-bound CHMP4 (Sun et al., 2015b). ALG-2 knockdown inhibited ALIX-supported MVB sorting and degradation of activated EGFR, but did not affect ESCRT-mediated cytokinetic abscission or retroviral budding (Sun et al., 2015a). These findings identify ALG-2 as a critical regulator of ALIX in calcium-dependent ESCRT processes and predict that a different

mechanism activates ALIX for it to function in calcium-independent ESCRT-mediated processes.

The *Xenopus* ortholog of ALIX, Xp95, is phosphorylated both at the conserved tyrosine residue (Y318) within Patch 2 of the Bro1 domain (Che et al., 1999) and at multiple sites within the N-terminal half of the PRD (nPRD) during *Xenopus* oocyte maturation (Dejournett et al., 2007). Since these phosphorylations also occur in ALIX (Dejournett et al., 2007; Schmidt et al., 2005), phosphorylation of one or both of the intramolecular interaction sites may transform ALIX from closed to open conformation. In this study, we demonstrated that mitotic phosphorylation of cytosolic ALIX at the intramolecular interaction site within the nPRD transforms ALIX from closed to open conformation. We also showed that this activating phosphorylation of ALIX is required for ALIX to function in cytokinetic abscission and equine infectious anemia virus (EIAV) budding but not in MVB sorting of activated EGFR.

## RESULTS

### Cytosolic ALIX Changes from Closed to Open Conformation during M Phase Induction

As illustrated in Figure 1A, the anti-ALIX antibody 1A3 recognizes the Patch 2/Src docking site in the Bro1 domain, and the anti-ALIX antibody 2H12 recognizes the F676 pocket/the viral GAG docking site in the V domain. Because the intramolecular interaction of ALIX renders these two partner protein docking sites inaccessible, 1A3 and 2H12 only immunoprecipitate opened ALIX. In contrast, the anti-ALIX antibodies 3A9 and 1A12 recognize conformation-insensitive epitopes within the V domain and thus immunoprecipitate both opened and closed ALIX (Zhou et al., 2010). We used immunoprecipitation (IP) with 1A3 or 2H12 to determine whether cytosolic ALIX undergoes a conformational change when HEK293 cells proceed from interphase (I) to mitosis (M).

Asynchronously growing cells (>95% in I, called I cells) or mitotically arrested cells (>80% in M, called M cells) were extracted with a detergent-free buffer to isolate cytosolic proteins without affecting the intramolecular interaction of ALIX (Zhou et al., 2008, 2009). ATP and the PP1/PP2A inhibitor microcystin were added to the extraction buffer for M cells to stabilize the M phase status of the extracts. Immunoblotting (IB) of I cell extracts (IE) or M cell extracts (ME) with the mitotic phosphoprotein monoclonal antibody 2 (MPM-2) (Wu et al., 2010) demonstrated a dramatically increased level of protein phosphorylation in M cells. ALIX IB showed that levels of ALIX are similar between I and M cells (Figure 1B). IP results showed that 1A12 and 3A9 immunoprecipitated ALIX from both IE and ME, whereas 1A3 and 2H12 immunoprecipitated ALIX only from ME (Figure 1C), indicating a conformational change of ALIX during mitotic entry. To determine whether the difference in ALIX conformation between IE and ME was due to different buffer conditions, we prepared both IE and ME in the presence of ATP and microcystin and performed parallel IP with 2H12 and 3A9. Under the same buffer conditions, 2H12 immunoprecipitated a trace amount of ALIX from IE but a high level of ALIX from ME (Figure S1A). The trace amount of 2H12-immunoprecipitable ALIX in IE could be from a small percentage of mitotic cells present in I cells. Together, these re-

sults indicate that ALIX changes from closed to open conformation during mitotic entry.

To characterize opened ALIX in M cells, we examined ALIX interaction with ectopically expressed CHMP4b, endogenous TSG101, and GST-Src. Both FLAG-CHMP4b and TSG101 coimmunoprecipitated with ALIX in ME but not in IE (Figures 1D and 1E). GST-Src also specifically pulled down ALIX from ME (Figure 1F). These results indicate that the opened cytosolic ALIX in mitotic cells is able to interact with multiple partner proteins.

We previously showed that relieving the intramolecular interaction of cytosolic ALIX promotes CHMP4-mediated ALIX association with the membrane in I cells (Sun et al., 2015a; Zhou et al., 2010). To determine whether this also occurs in M cells, we fractionated the post nuclear supernatant (PNS) of crude cell lysates from I or M cells by membrane flotation centrifugation. The distribution of ALIX and CHMP4b between membrane and soluble protein fractions was similar between I and M cells (Figure S1C), suggesting that membrane-bound CHMP4 in M cells cannot interact with newly opened cytosolic ALIX.

To determine whether Xp95 undergoes a conformational change during oocyte maturation, we immunoprecipitated Xp95 from interphase-arrested *Xenopus* oocyte extracts (IOE) or M phase-arrested *Xenopus* egg extracts (MEE), which were also prepared in the absence of detergent, with 1A3 and 1A12. While 1A12 immunoprecipitated Xp95 from both IOE and MEE, 1A3 specifically immunoprecipitated Xp95 from MEE (Figure 1G), indicating that the M phase-associated conformational change of cytosolic ALIX is a conserved phenomenon that applies to both mitotic and meiotic cycles.

To determine the role of protein phosphorylation in the conformational change of ALIX during mitotic entry, we treated ME with calf intestinal alkaline phosphatase (CIP) and determined the effect on ALIX conformation. CIP treatment both eliminated MPM-2 reactivity (Figure 1H) and reversed 1A3 immunoprecipitability of ALIX (Figures 1I and S1B), indicating that protein phosphorylation plays a critical role in the conformational change of ALIX during mitotic entry. Interestingly, if GST-CHMP4b or myc-TSG101 was added to ME before the CIP treatment, the CIP-induced reversal of the 1A3 immunoprecipitability became partial (Figures 1I and S1B), indicating that the acquired intermolecular interaction of ALIX decreases the probability of reforming the intramolecular interaction of ALIX after dephosphorylation of mitotic phosphoproteins.

### MEE Treatment of ALIX$_{nPRD}$ Inhibits Its Interaction with ALIX$_{Bro1}$

To define the protein phosphorylation that relieves the intramolecular interaction of ALIX in mitotic cells, we first incubated GST-tagged ALIX$_{1-746}$, which contains both of the intramolecular interaction sites (Figure 2A) (Zhou et al., 2010), with IOE, MEE, or MEE plus CIP, and immunoprecipitated the end products with 3A9 or 2H12. 3A9 immunoprecipitated high levels of GST-ALIX$_{1-746}$ under all three conditions, whereas 2H12 immunoprecipitated a readily detectable level of GST-ALIX$_{1-746}$ only after its treatment with MEE (Figure 2B). That the MEE induces an open conformation of GST-ALIX$_{1-746}$ was further confirmed by GST-ALIX$_{1-746}$ pull-down of FLAG-CHMP4b (Figure 2C).

To identify the ALIX domain through which MEE treatment relieves the intramolecular interaction of ALIX, we produced
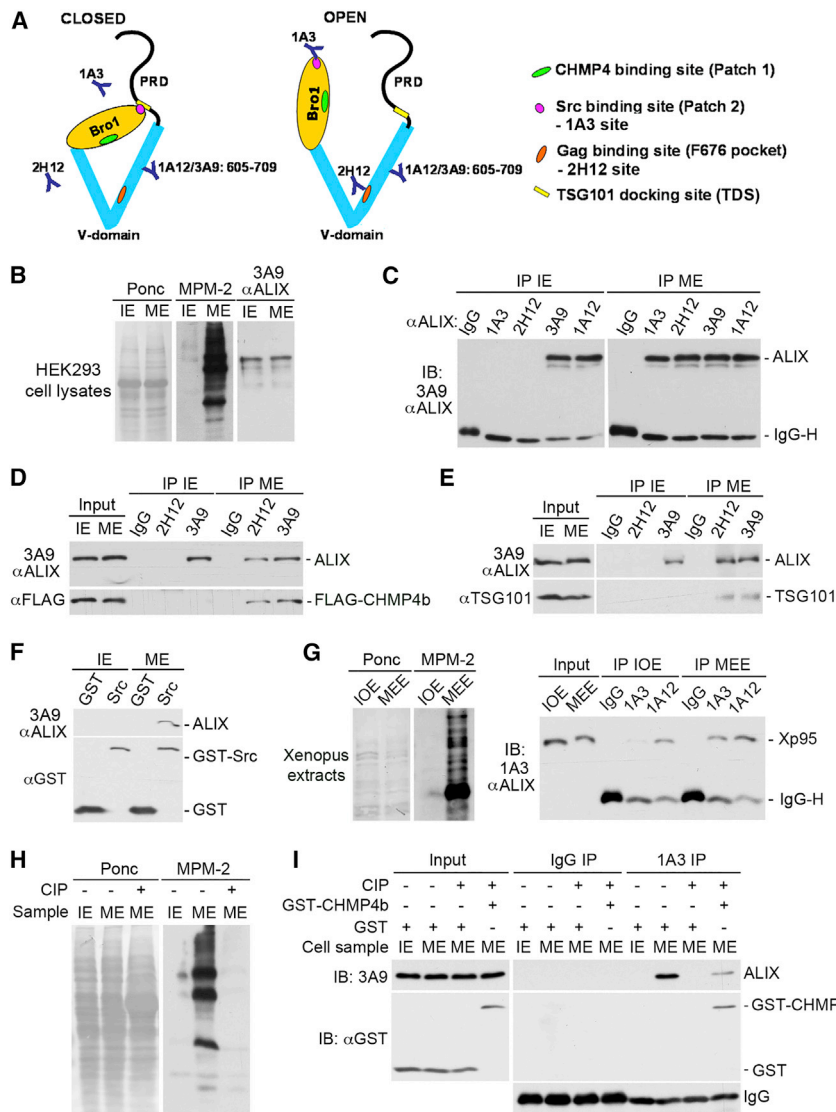
**Figure 1. Cytosolic ALIX Changes from Closed to Open Conformation during M Phase Induction**

(A) Schematic illustration of the closed and open conformations of ALIX.

(B) IB of IE and ME with MPM-2 and 3A9 after Ponceau S (Ponc) staining.

(C–E) IP of IE and ME with the indicated antibodies, followed by IB with the indicated antibodies.

(F) Incubation of IE and ME with GST or GST-Src, followed by IB of bound proteins with the indicated antibodies.

(G) IB of IOE or MEE with MPM-2, and IP of IOE or MEE with the indicated antibodies, followed by IB with 1A3.

(H) IB of IE, ME, and CIP-treated ME with MPM-2.

(I) ME was first incubated with GST or GST-CHMP4b at 4°C for 2 hr and then treated with CIP. IE, ME, and the two samples of differently treated ME were immunoprecipitated with the indicated antibodies, followed by IB with the indicated antibodies. See also Figure S1.

## S718-S721 Phosphorylation Inhibits the ALIX$_{nPRD}$ Interaction with ALIX$_{Bro1}$

The nPRD of Xp95 is phosphorylated at multiple sites in mature oocytes (Dejour-nett et al., 2007). Sequence alignment of the nPRD of ALIX with that of Xp95 showed that the nPRD contains seven conserved S/T residues, two of which (S718 and S721 in ALIX) localize at or near the TDS at 717–720 (Figure 3A). We thus determined whether MEE phosphorylates the S718 and S721 residues in ALIX$_{nPRD}$.

The phospho-(Ser/Thr) PKD substrate antibody #4381 from Cell Signaling Technology detects peptides containing a phospho-S/T residue with arginine at the −3 position and leucine at the −5 position, preferring proline at the −1 position. Since the S718 context meets all of these criteria and #4381 preferentially detected a polypeptide about the size of ALIX in ME (Figure S2A), we used #4381 to determine whether MEE phosphorylates the S718 residue in ALIX$_{nPRD}$. MEE treatment of the wild-type (WT) but not the S718A-S721A (S2A) mutant form of GST-ALIX$_{nPRD}$ or myc-ALIX$_{nPRD}$ generated reactivity to #4381, as determined by IB or IP (Figure 3B). We also generated rabbit polyclonal antibodies against a synthetic ALIX peptide that is phosphorylated at both S718 and S721 and observed that the antibodies, named the anti-pS2 antibody (αpS2), also preferentially recognized a polypeptide about the size of ALIX in ME (Figure S2B). As observed with #4381, αpS2 specifically recognized WT but not S2A GST-ALIX$_{nPRD}$ or myc-ALIX$_{nPRD}$ upon MEE treatment (Figure 3C). The recognition was sensitive to CIP treatment (Figure S2C). Incubation of WT but not S2A GST-ALIX$_{nPRD}$ with progesterone-matured oocyte extracts, freshly prepared in the absence of microcystin, also generated reactivity to αpS2 in a CIP-sensitive manner (Figures
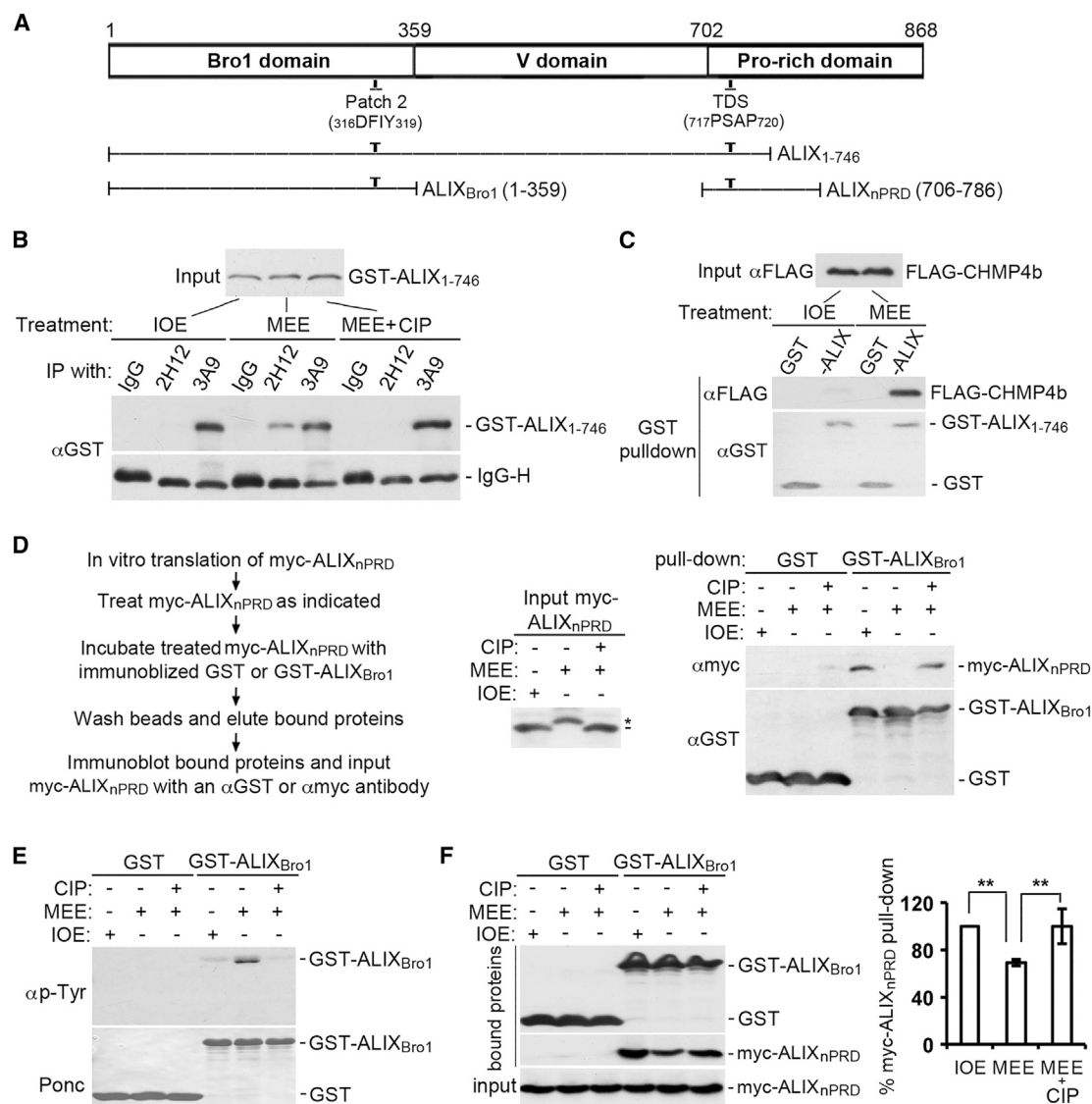
GST-ALIX$_{Bro1}$ and myc-ALIX$_{nPRD}$ (Figure 2A) and verified their interaction. We then incubated the in vitro transcription-linked-translation (TNT) product of myc-ALIX$_{nPRD}$ with IOE, MEE, or MEE plus CIP as diagrammed (Figure 2D, left) and determined the effect on myc-ALIX$_{nPRD}$ interaction with GST-ALIX$_{Bro1}$. Treating myc-ALIX$_{nPRD}$ with MEE but not with IOE or MEE plus CIP induced a gel mobility shift (Figure 2D, middle). Accordingly, GST-ALIX$_{Bro1}$ pulled down myc-ALIX$_{nPRD}$ treated with IOE or MEE plus CIP but not with MEE (Figure 2D, right). We also incubated GST-ALIX$_{Bro1}$ with IOE, MEE, or MEE plus CIP, examined the tyrosine phosphorylation of the washed substrate, and determined its interaction with myc-ALIX$_{nPRD}$. Treating GST-ALIX$_{Bro1}$ with MEE but not with IOE or MEE plus CIP generated immunoreactivity to anti-phosphotyrosine antibodies (Figure 2E). However, the MEE treatment only moderately reduced the ability of GST-ALIX$_{Bro1}$ to interact with myc-ALIX$_{nPRD}$ (Figure 2F). Together, these results indicate that the MEE treatment relieves the intramolecular interaction of ALIX mainly through targeting the nPRD.

**Figure 2. MEE Treatment of ALIX_nPRD Inhibits Its Interaction with ALIX_Bro1**

(A) Schematic illustration of the regions of ALIX that comprise the three structural domains and the ALIX fragments used in this study.

(B) GST-ALIX$_{1-746}$ was phosphorylated with IOE, MEE, or MEE plus CIP, and end products were immunoprecipitated with the indicated antibodies, followed by IB with αGST.

(C) GST or GST-ALIX$_{1-746}$ was phosphorylated with IOE or MEE, and then absorbed onto GSH beads. The washed beads were used to pull down FLAG-CHMP4b in IE. IB of input and bound proteins with the indicated antibodies.

(D) Left: experimental flowchart. Middle: IB of input myc-ALIX$_{nPRD}$; the short line and the asterisk indicate the start and shift positions of myc-ALIX$_{nPRD}$, respectively. Right: IB of bound proteins.

(E) Phosphorylation of GST or GST-ALIX$_{Bro1}$ with IOE, MEE, or MEE plus CIP, followed by IB of washed proteins with αphosphotyrosine (p-Tyr).

(F) Washed GST or GST-ALIX$_{Bro1}$ proteins in (E) were tested for interaction with myc-ALIX$_{nPRD}$ by GST pull-down (n = 3 ± SD). **0.001 ≤ p < 0.01.

S2D–S2F). Collectively, these results indicate that MEE phosphorylates S718-S721 in ALIX$_{nPRD}$.

To determine whether the phosphorylation of ALIX$_{nPRD}$ at S718-S721 is required for MEE-induced inhibition of the ALIX$_{nPRD}$ interaction with ALIX$_{Bro1}$, we produced a phosphomimetic form of myc-ALIX$_{nPRD}$ on S718-S721 (S718D-S721D, S2D) and a control phosphodefective form of myc-ALIX$_{nPRD}$ on S712-S729 (S712A-S729A, S2A−). We then incubated S2A, S2A−, or S2D myc-ALIX$_{nPRD}$ with IOE, MEE, or MEE plus CIP,

and characterized their interaction with GST-ALIX$_{Bro1}$. None of the double mutations eliminated the gel mobility shift of myc-ALIX$_{nPRD}$ in MEE (Figure 3D, left), consistent with previous results (Dejournett et al., 2007). However, while S2A myc-ALIX$_{nPRD}$ interacted with GST-ALIX$_{Bro1}$ under all three conditions, S2D myc-ALIX$_{nPRD}$ did not do so under any of the three conditions. Only S2A− myc-ALIX$_{nPRD}$ interacted with GST-ALIX$_{Bro1}$ upon incubation with IOE or MEE plus CIP but not with MEE (Figure 3D, right). These results indicate that S718-S721 phosphorylation is
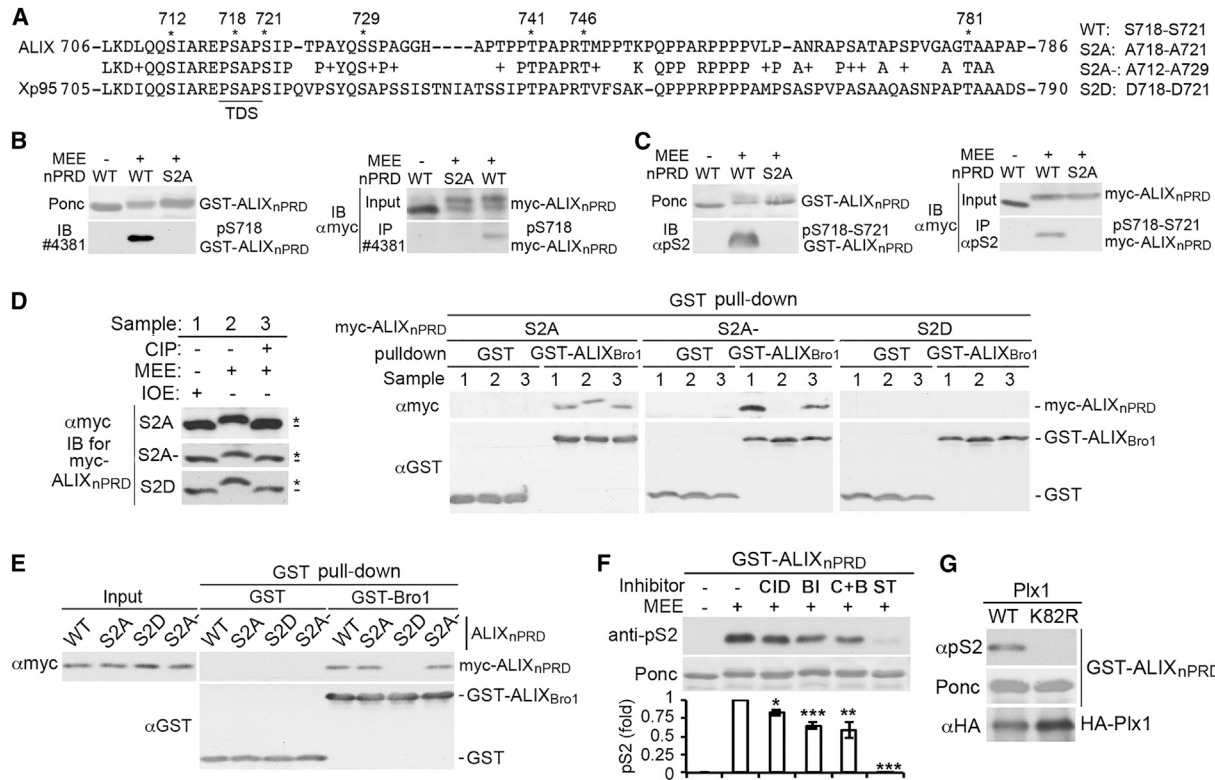
**Figure 3. S718-S721 Phosphorylation Inhibits the ALIX$_{nPRD}$ Interaction with ALIX$_{Bro1}$**

(A) Sequence alignment of the ALIX$_{nPRD}$ with the Xp95 $_{nPRD}$; the conserved S/T sites are indicated with asterisks.

(B and C) Left: IB of mock-treated or MEE phosphorylated GST-ALIX$_{nPRD}$ with #4381 (B) or αpS2 (C). Right: dIP of mock-treated or MEE phosphorylated myc-ALIX$_{nPRD}$ with #4381 (B) or αpS2 (C), followed by IB with αmyc.

(D) GST or GST-ALIX$_{Bro1}$ pull-down of the indicated forms of myc-ALIX$_{nPRD}$ after their treatment with IOE, MEE, or MEE plus CIP, followed by IB with the indicated antibodies.

(E) Pull-down of the indicated forms of myc-ALIX$_{nPRD}$ with GST or GST-ALIX$_{Bro1}$, followed by IB with the indicated antibodies.

(F) GST-ALIX$_{nPRD}$ was mock treated or phosphorylated at 22°C for 1 hr with MEE in the presence or absence of CID755673 (CID), BI-2536 (BI), both inhibitors (C + B), or staurosporine (ST). After the substrate was immobilized onto GSH beads and washed, bound proteins were probed with αpS2 to determine the level of S718-S721 phosphorylation (n = 3 ± SD). *$0.01 \leq p < 0.05$; **$0.001 \leq p < 0.01$; ***$p < 0.001$.

(G) Phosphorylation of GST-ALIX$_{nPRD}$ with HA-Plx1, followed by IB of the substrate with αpS2.

required for MEE-induced inhibition of the ALIX$_{nPRD}$ interaction with ALIX$_{Bro1}$.

S718-S721 phosphorylation may directly inhibit the ALIX$_{nPRD}$ interaction with ALIX$_{Bro1}$ through phosphorylation-produced negative charges or by generating a docking site for a cofactor that prevents the ALIX$_{nPRD}$ interaction with ALIX$_{Bro1}$. To distinguish between these two possibilities, we determined the interaction of different mutant forms of myc-ALIX$_{nPRD}$ with GST-ALIX$_{Bro1}$ in the absence of *Xenopus* extracts. GST-ALIX$_{Bro1}$ pulled down WT, S2A, and S2A− myc-ALIX$_{nPRD}$ but not S2D myc-ALIX$_{nPRD}$ (Figure 3E), favoring the direct inhibition of the ALIX$_{nPRD}$ interaction with ALIX$_{Bro1}$ by S718-S721 phosphorylation.

The S718 context fits with the phosphorylation consensus sequences for PKD and PLK1. Since both PKD and PLK1 are activated in mitotic cells (Golsteyn et al., 1995; Kienzle et al., 2013), we determined whether PKD and/or PLK1 are the major kinases in MEE that phosphorylate S718-S721. GST-ALIX$_{nPRD}$ was phosphorylated with MEE in the presence or absence of the PKD inhibitor CID755673 and/or the PLK1 inhibitor BI-2536 or

the pan kinase inhibitor staurosporine, and the washed substrate was probed with αpS2. The pan kinase inhibitor dramatically inhibited the phosphorylation of GST-ALIX$_{nPRD}$. In contrast, the PKD and PLK1 inhibitors reduced the phosphorylation to 83% and 65% of the control level, respectively, and their combined use reduced the phosphorylation to 59% of the control level (Figure 3F). We also phosphorylated GST-ALIX$_{nPRD}$ with purified *Xenopus* PLK1 (Plx1). WT but not a catalytically inactive (K82R) Plx1 generated immunoreactivity to αpS2 (Figure 3G). These results indicate that PKD and PLK1 are among the protein kinases in MEE that phosphorylate S718-S721 in ALIX$_{nPRD}$.

### S718-S721 Phosphorylation Relieves the Intramolecular Interaction of ALIX

We determined the recognition of ALIX from I and M cells by #4381 and αpS2 to establish whether ALIX is phosphorylated at S718-S721 in M cells. Denatured IE or ME (dIE or dME) were prepared with 1% SDS to preserve the phosphorylation status, and denaturing immunoprecipitation (dIP) was performed after neutralization of SDS with NP-40. Both phosphospecific
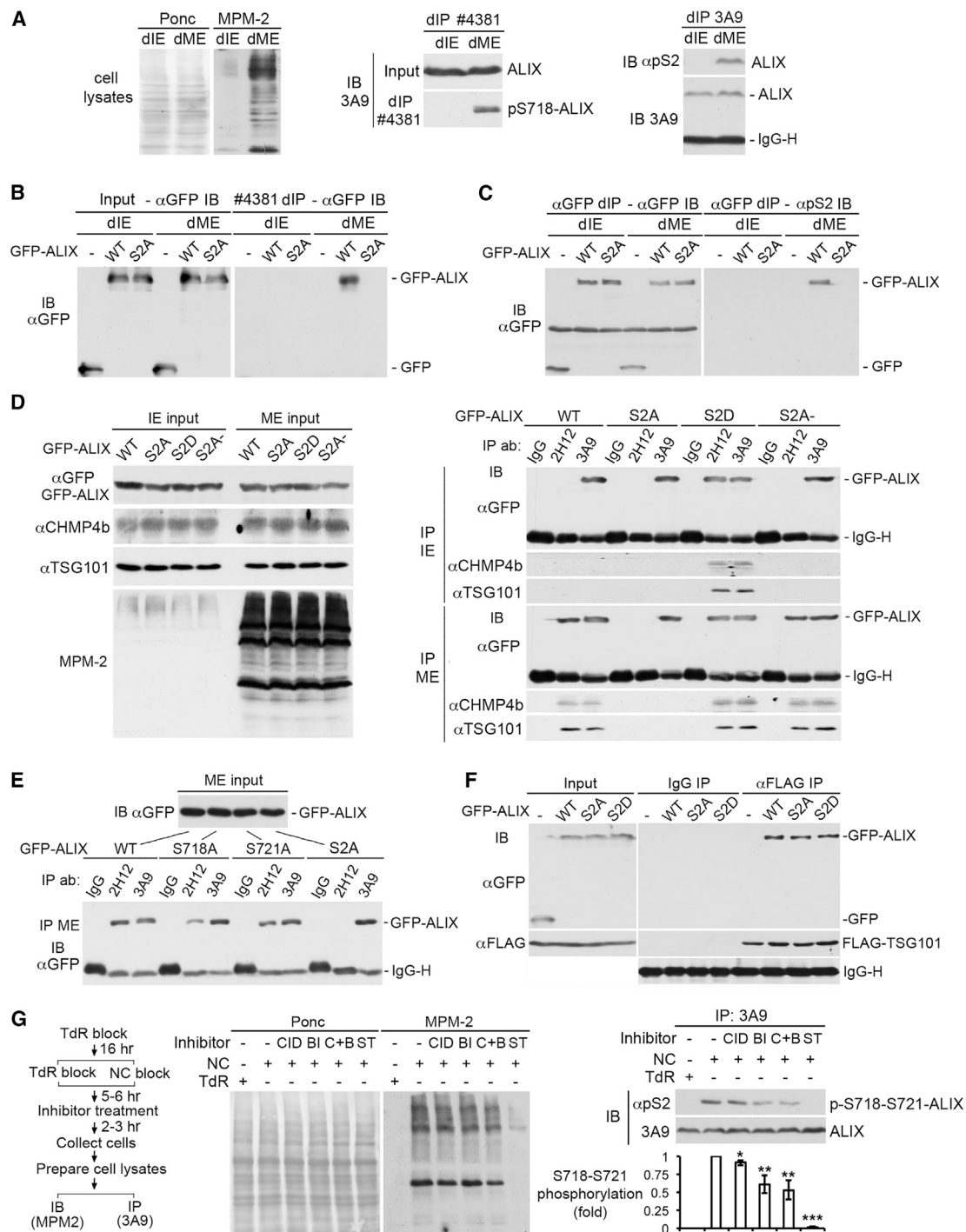
**Figure 4. S718-S721 Phosphorylation Relieves the Intramolecular Interaction of ALIX**

(A) Left: IB of dIE and dME with MPM-2. Middle: dIP with #4381, followed by IB with 3A9. Right: dIP with 3A9, followed by IB with 3A9 and αpS2.

(B) dIP of IE and ME from cells ectopically expressing WT or S2A GFP-ALIX with #4381, followed by IB with αGFP.

(C) dIP of the IE and ME samples in (B) with αGFP, followed by IB with αGFP and αpS2.

(D) Left: IB of IE and ME from cells ectopically expressing the indicated forms of GFP-ALIX with the indicated antibodies. Right: IP of the IE or ME samples with IgG or the indicated αALIX, followed by IB with the indicated antibodies.

(E) IP of ME from cells ectopically expressing the indicated forms of GFP-ALIX with IgG or the indicated αALIX, followed by IB of input proteins and immunocomplexes with αGFP.

*(legend continued on next page)*

antibodies differentially recognized ALIX from M cells (Figure 4A). When WT or S2A GFP-ALIX was expressed in HEK293 cells, both #4381 (Figure 4B) and αpS2 (Figure 4C) recognized WT GFP-ALIX but not S2A GFP-ALIX in ME, confirming that the antibody recognition was due to S718-S721 phosphorylation.

To determine the effect of S718-S721 phosphorylation on the intramolecular interaction of ALIX, we ectopically expressed WT, S2A, S2D, or S2A− GFP-ALIX in HEK293 cells and probed their conformation by IP with 2H12. 2H12 immunoprecipitated WT and S2A− GFP-ALIX from ME but not IE, S2A GFP-ALIX from neither IE nor ME, but S2D GFP-ALIX from both IE and ME. IB of the immunocomplexes with αCHMP4b and αTSG101 showed that, in all cases, the 2H12 immunoprecipitability correlated the GFP-ALIX interaction with CHMP4b and TSG101 (Figure 4D). These results indicate that S718-S721 phosphorylation is responsible for relieving the intramolecular interaction of cytosolic ALIX in M cells.

To determine whether phosphorylation of both the S718 and S721 residues is required for relieving the intramolecular interaction of ALIX, we expressed the S718A and S721A single mutant forms of GFP-ALIX, and probed their conformation in M cells by IP with 2H12. While 2H12 did not immunoprecipitate S2A GFP-ALIX, it immunoprecipitated the S718A and S721A single mutant forms of GFP-ALIX at ∼40% and ∼70% of the level of WT GFP-ALIX, respectively (Figure 4E). These results indicate that phosphorylation of both the S718 and S721 residues is required to relieve the intramolecular interaction of ALIX most efficiently.

The 717–720 motif is also critically involved in ALIX interaction with TSG101 (Carlton et al., 2008). Since ALIX differentially interacted with TSG101 in mitotic cells (Figure 1E), we speculated that the phosphorylation of this dual protein interaction site specifically regulates the intramolecular interaction of ALIX without affecting ALIX interaction with TSG101. To test this possibility, we co-expressed FLAG-TSG101 with WT, S2A, or S2D GFP-ALIX in HEK293 cells and determined the FLAG-TSG101 interaction with each form of GFP-ALIX in IE in the presence of 1% Triton X-100, which disrupts the intramolecular interaction of ALIX (Zhou et al., 2008). FLAG-TSG101 interacted with both mutant forms of GFP-ALIX as efficiently as with WT GFP-ALIX (Figure 4F), supporting our hypothesis.

To determine the role of PKD and/or PLK1 in S718-S721 phosphorylation in M cells, we accumulated cells in mitosis in the presence or absence of kinase inhibitors and probed ALIX phosphorylation with αpS2. As anticipated, the pan kinase inhibitor inhibited both mitotic entry and S718-S721 phosphorylation. In contrast, the PKD inhibitor slightly inhibited ALIX phosphorylation without affecting mitotic entry; the PLK1 inhibitor reduced ALIX phosphorylation to 75% of the control level without affecting mitotic entry; and the combined use of the two inhibitors reduced ALIX phosphorylation to 61% of the control level without affecting mitotic entry (Figure 4G). These results indicate that PLK1, and likely also PKD, contribute to S718-S721 phosphorylation in M cells.

## S718-S721 Phosphorylation Is Required for ALIX to Function in Cytokinetic Abscission

Both ALIX and TSG101 interact with cep55 at the midbody and promote ESCRT-III assembly through recruiting CHMP4 (Carlton and Martin-Serrano, 2007; Morita et al., 2007). Since the cep55 interaction site in ALIX localizes at 801–806 (Carlton et al., 2008), which is outside the region required for the intramolecular interaction of ALIX (Zhou et al., 2010), S718-S721 phosphorylation is unlikely to be required for ALIX localization at the midbody but may be required for ALIX to recruit CHMP4 to the midbody. To test these predictions, we first examined the effect of ALIX knockdown on the midbody localization of mCherry (mCh)-tagged CHMP4b or TSG101 in HeLa cells. Consistent with the current understanding, ALIX knockdown inhibited the midbody localization of mCh-CHMP4b in >70% of the cells examined but had little effect on the midbody localization of mCh-TSG101 (Figures S3A and S3B). We then compared the abilities of different forms of siRNA-insensitive GFP-ALIX (GFP-ALIX*) to rescue the defect of the midbody localization of mCh-CHMP4b. All forms of GFP-ALIX* examined were able to localize at the midbody. However, while WT and S2A− GFP-ALIX* restored the midbody localization of mCh-CHMP4b to near control levels, S2A GFP-ALIX* did not (Figure 5A). These results demonstrate that S718-S721 phosphorylation is required for ALIX to recruit CHMP4 to the midbody.

The above results predicted that S718-S721 phosphorylation is required for ALIX to function in cytokinetic abscission. To test this, we compared the abilities of WT, S2A, and S2A− GFP-ALIX* to rescue the defect of ALIX knockdown cells in cytokinetic abscission. Consistent with previous observations (Carlton and Martin-Serrano, 2007; Morita et al., 2007), ALIX knockdown increased the percentages of midbody-stage and multinucleated cells from <2% to ∼14% and ∼17%, respectively (Figure S3C). While the expression of WT or S2A− GFP-ALIX* reduced the percentage of midbody-stage or multinucleated cells to near control levels, the expression of S2A GFP-ALIX* did not rescue the cytokinetic abscission defect despite its ability to localize to the midbody (Figure 5B). The expression of S2A GFP-ALIX* in control knockdown cells did not generate any phenotypes in cytokinetic abscission (data not shown). The intracellular bridge in S2A GFP-ALIX*-expressing cells appeared largely normal without the secondary ingression. These results supported our prediction.

Previous studies indicated that ∼50% of ALIX knockdown cells had anti-tubulin staining persisting through the Flemming body, whereas ∼10% of control cells had such aberrant midbodies (Carlton et al., 2008). Under our experimental conditions, however, only 3% and 12% of control and ALIX knockdown cells had aberrant midbodies, respectively (Figure S3D). The discrepancy of our observation with that in previous studies could be due to different culture conditions, which may affect the rate of conversion of midbody-stage cells to multinucleated cells.

(F) IP of IE from cells ectopically coexpressing FLAG-TSG101 and GFP or the indicated forms of GFP-ALIX with αFLAG in the presence of 1% Triton X-100, followed by IB of input proteins and immunocomplexes with the indicated antibodies.
(G) Left: experimental flowchart for cell treatments. Middle: IB of IE and ME from collected cells with MPM2. Right: determination of S718-S721 phosphorylation by dIP with 3A9, followed by IB with 3A9 and αpS2 (n = 3 ± SD). *0.01 ≤ p < 0.05; **0.001 ≤ p < 0.01; ***p < 0.001. See also Figure S2.
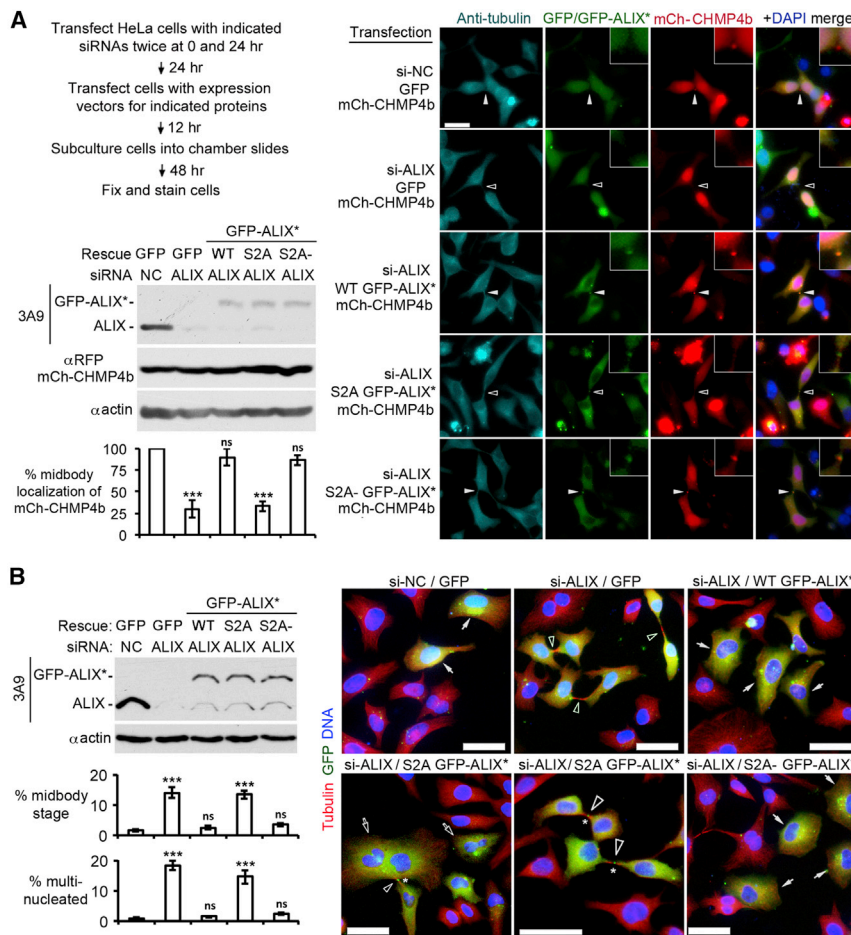
## A



Transfect HeLa cells with indicated siRNAs twice at 0 and 24 hr
↓ 24 hr
Transfect cells with expression vectors for indicated proteins
↓ 12 hr
Subculture cells into chamber slides
↓ 48 hr
Fix and stain cells

## B

(A) HeLa cells were transfected with the indicated agents and cultured as diagrammed, followed by IB of cell lysates with the indicated antibodies. Fixed cells were stained with αtubulin and αGFP, and GFP-mCherry double-positive cells were scored for the midbody localization of mCh-CHMP4b (n = 3 ± SD). Solid and open arrowheads in the representative images indicate the presence or absence of mCh-CHMP4b at the midbody, respectively. Enlargements (3×) depict the midbody area; scale bar, 50 μm.

(B) HeLa cells were transfected with the indicated agents and cultured as in (A), followed by IB of cell lysates with the indicated antibodies. Fixed cells were stained with αtubulin and αGFP, and GFP-positive cells were scored for midbody stage or multinucleation (n = 3 ± SD). Solid and open arrows in representative images indicate GFP-positive mononucleated and multinucleated cells, respectively; open arrowheads indicate midbodies between GFP-positive cells; and the asterisks indicate the midbody localization of GFP-ALIX*.

ns, not significant. ***p < 0.001. Scale bar, 50 μm. See also Figure S3.

generate a significant pool of opened ALIX. We then determined the ability of different forms of GFP-ALIX* to rescue the defect of ALIX knockdown cells in EIAV budding. While WT and S2A− GFP-ALIX rescued the defect, S2A GFP-ALIX did not (Figure 6D), indicating that S718-S721 phosphorylation is required for ALIX to function in EIAV budding.

To determine whether S718-S721 phosphorylation that supports EIAV budding occurs in I or M cells, we determined the effect of mitotic or S phase arrest on EIAV budding. Arresting cells in mitosis greatly inhibited EIAV budding (Figure 6E), whereas arresting cells in S phase had no effect (Figure 6F), indicating that S718-S721 phosphorylation that supports EIAV budding occurs in interphase cells.

### S718-S721 Phosphorylation Does Not Affect the Function of ALIX in MVB Sorting of Activated EGFR

Our previous studies demonstrated that calcium-dependent ALG-2 interaction with ALIX relieves the intramolecular interaction of ALIX in EGF-stimulated cells and promotes MVB sorting of activated EGFR (Sun et al., 2015a). To determine whether S718-S721 phosphorylation may cooperate with the ALG-2-dependent mechanism to fully activate the MVB sorting function of ALIX, we first determined the effect of the S2A mutation on ALIX association with the membrane, which indicates ALIX interaction with membrane-bound CHMP4. ALIX with deletion of the ALG-2 binding site (ΔPxY), which inhibits CHMP4-dependent ALIX association with the membrane, was used as a control (Sun et al., 2015a). As previously observed, EGF stimulation increased the membrane-associated WT GFP-ALIX by ∼3-fold,

### S718-S721 Phosphorylation Is Required for ALIX to Function in EIAV Budding

EIAV budding requires ALIX interaction with both CHMP4b and the GAG protein p9 (Strack et al., 2003; von Schwedler et al., 2003). Since relieving the intramolecular interaction of ALIX is required for both events (Zhou et al., 2010), EIAV budding is an ideal model system for defining the role of S718-S721 phosphorylation in retroviral budding. GST-p9 pulled down ALIX from ME but not IE (Figure 6A), indicating that the phosphorylation-induced open conformation of ALIX supports ALIX interaction with p9. IP with 1A3 showed that the prior incubation of ME with GST-p9 partially sustained the open conformation of ALIX after ME dephosphorylation (Figure 6B). GST-p9 also sustained the open conformation of GFP-ALIX when GFP-ALIX was first phosphorylated by MEE and then dephosphorylated by IOE (Figure S4). These results indicate that the p9 interaction with phosphorylated ALIX helps sustain the open conformation of ALIX after ALIX dephosphorylation.

To determine the role of S718-S721 phosphorylation in EIAV budding, we first co-expressed WT, S2A, or S2A− GFP-ALIX with an infection-defective EIAV in HEK293 cells and examined their conformation by IP with 1A3. 1A3 immunoprecipitated a readily detectable level of WT or S2A− GFP-ALIX but not S2A GFP-ALIX (Figure 6C), indicating that S718-S721 phosphorylation is required for EIAV-expressing cells to
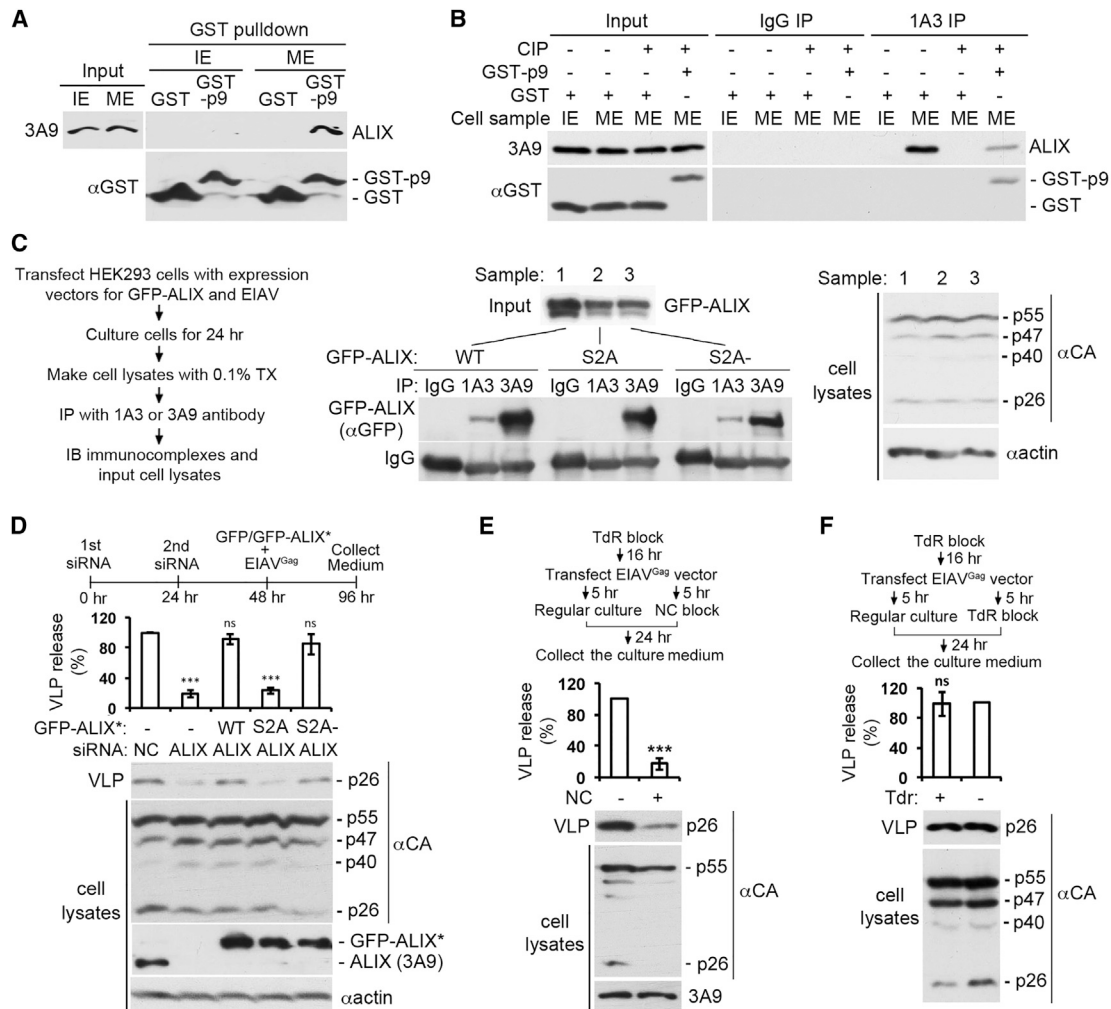
**Figure 6. S718-S721 Phosphorylation Is Required for ALIX to Function in EIAV Budding**

(A) Incubation of GST or GST-p9 with IE or ME, followed by IB of input and bound proteins with the indicated antibodies.

(B) ME was first incubated with GST or GST-p9 at 4°C for 2 hr, and then treated with CIP. IE, ME, and the two samples of differently treated ME were immunoprecipitated with IgG or 1A3, followed by IB with the indicated antibodies.

(C) Left: experimental flowchart. Middle: IP of cell lysates with the indicated antibodies, followed by IB with αGFP. Right: IB of cell lysates with the indicated antibodies.

(D–F) HEK293 cells were processed as diagrammed. IB of VLPs and cell lysates with the indicated antibodies. Relative levels of the VLP production were determined (n = 3 ± SD). ns, not significant. ***p < 0.001. See also Figure S4.

and ΔPxY GFP-ALIX barely associated with the membrane irrespective of EGF stimulation. However, S2A GFP-ALIX behaved similarly as WT GFP-ALIX (Figures 7A and S5A), indicating that S718-S721 phosphorylation does not affect CHMP4-dependent ALIX association with the membrane.

We then determined the ability of S2A GFP-ALIX to rescue the defect of ALIX knockdown cells in MVB sorting of activated EGFR by the Proteinase K protection assay used in our previous studies (Sun et al., 2015a, 2015b). Consistent with our previous results, ALIX knockdown reduced the percentage of protected EGFR from ~60% to ~15%. Importantly, both S2A and S2A– GFP-ALIX* rescued the inhibitory effect of ALIX knockdown as efficiently as WT GFP-ALIX* (Figure 7B, right). These results indicate that S718-S721 phosphorylation does not affect MVB sorting of activated EGFR.

Furthermore, we determined the ability of S2A GFP-ALIX to rescue the defect of ALIX knockdown cells in the timely silencing of activated EGFR. As previously observed, ALIX knockdown prevented the quick and dramatic inactivation of ERK1/2 after 10 min and sustained the ERK1/2 activation at 80% and 50% of the peak level at 30 min and 60 min, respectively. While the effect was rescued by the expression of WT GFP-ALIX* (Figure 7C), it was not rescued by the expression of ΔPxY GFP-ALIX* (Figure S5B). However, S2A GFP-ALIX* rescued the sustaining effect of ALIX knockdown on ERK1/2 activation (Figure 7D), indicating that S718-S721 phosphorylation does not affect the timely silencing of activated EGFR.

Finally, we determined the ability of S2A GFP-ALIX to reverse the retardation of ALIX knockdown cells in EGFR degradation
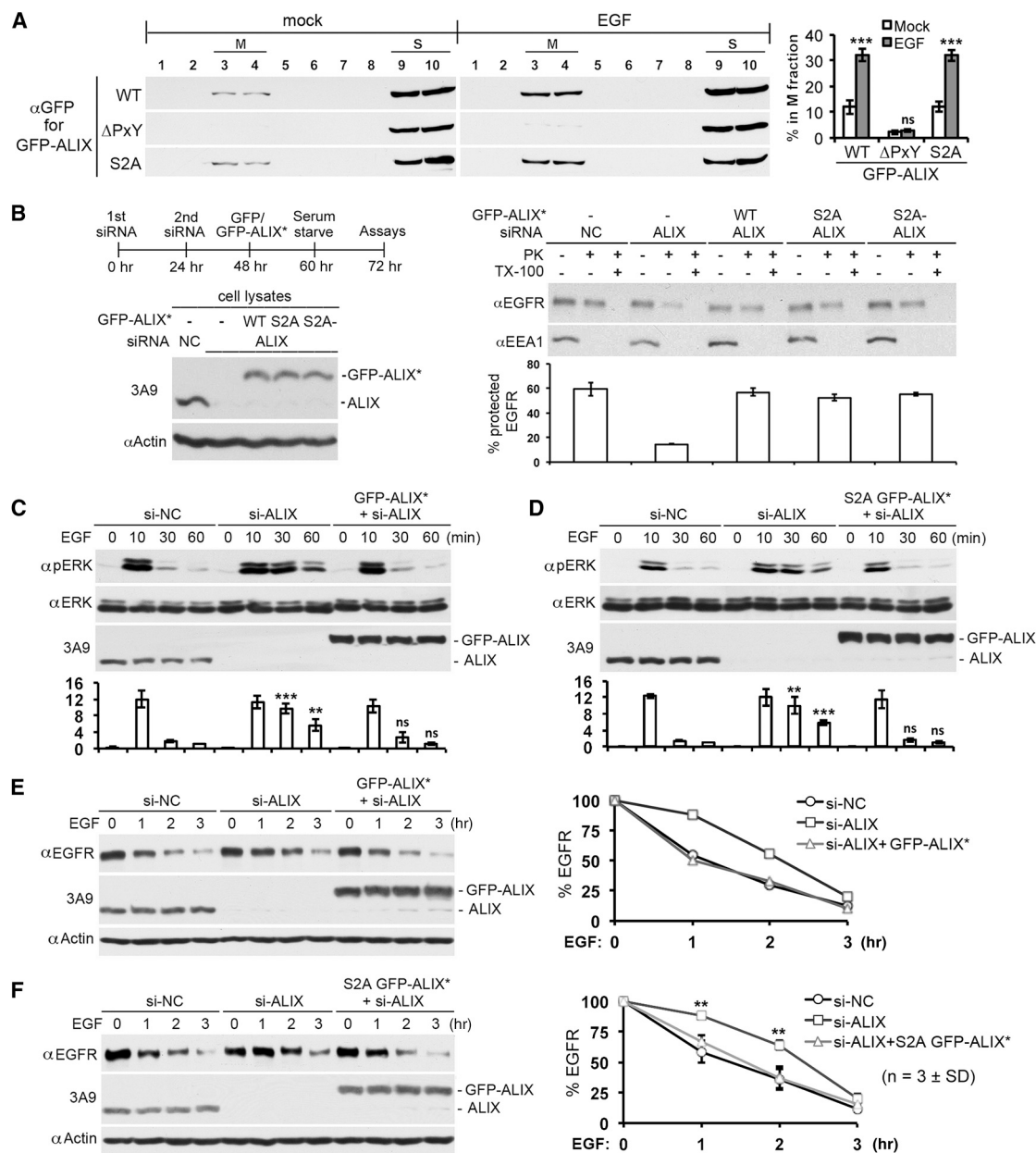
**Figure 7. S718-S721 Phosphorylation Does Not Affect the Function of ALIX in MVB Sorting of Activated EGFR**

(A) HEK293 cells ectopically expressing the indicated forms of GFP-ALIX were mock treated or stimulated with EGF for 1 hr, and the average percentage of each GFP-ALIX in the M fraction was determined by membrane flotation centrifugation of the PNS (n = 3 ± SD).

(B–F) Left: HEK293 cells were processed as diagrammed, and cell lysates were immunoblotted with the indicated antibodies. Right: cells were stimulated with EGF for 30 min and assayed for MVB sorting of activated EGFR by the Proteinase K protection assay (n = 2 ± data range). (C and D) Cells were stimulated with EGF for time indicated in minutes, and cell lysates were immunoblotted with the indicated antibodies. The relative levels of p-ERK were determined and normalized against the level of si-NC cells at 60 min (n = 3 ± SD). (E and F) Cells were stimulated with EGF for the time indicated in hours, and cell lysates were immunoblotted with the indicated antibodies. The percentages of remaining EGFR at different time points were determined.

ns, not significant. **$0.001 \leq p < 0.01$; ***$p < 0.001$. See also Figure S5.

under EGF continuous stimulation conditions. Consistent with our previous results (Sun et al., 2015b), ALIX knockdown retarded the 50% EGFR degradation from 1 hr to 2 hr, and the effect was rescued by the expression of WT GFP-ALIX* (Figure 7E) but not by ΔPxY GFP-ALIX* (Figure S5C). Importantly, the expression of S2A GFP-ALIX* rescued the retardation effect

of ALIX knockdown on EGFR degradation (Figure 7F), indicating that S718-S721 phosphorylation does not affect the timely degradation of activated EGFR.

Collectively, these results indicate that S718-S721 phosphorylation is not involved in generating opened ALIX that supports endolysosomal trafficking of activated EGFR.

## DISCUSSION

Mitosis is a special time in the cell cycle when a great portion of protein kinases are simultaneously activated (Daub et al., 2008) and thousands of proteins are robustly phosphorylated (Dephoure et al., 2008; Olsen et al., 2010). Although none of the known ESCRT-mediated processes occurs in mitosis, mitotic cells provide a unique platform to determine the role of protein phosphorylation in the regulation of ALIX conformation. Using this platform, we discovered that S718-S721 phosphorylation transforms ALIX from closed to open conformation and that multiple protein kinases, including PLK1 and likely also PKD, catalyze S718-S721 phosphorylation. Following this lead, we demonstrated that S718-S721 phosphorylation is required for ALIX to function in cytokinetic abscission and EIAV budding, but does not affect the function of ALIX in MVB sorting of activated EGFR. These findings identify the phosphorylation of the intramolecular interaction site within the nPRD as one of the major mechanisms that activates the ESCRT function of ALIX.

Since cells undergoing cytokinetic abscission have already biochemically entered interphase (Gershony et al., 2014), there seems to be a time lag between the activating phosphorylation of ALIX and the function of ALIX in cytokinetic abscission. However, accumulating evidence indicates that multiple activated mitotic kinases and phosphoproteins remain at the midbody much longer than the duration of mitosis. For example, the midbody was specifically recognized by the mitotic phosphoprotein monoclonal antibody MPM-2 (Davis et al., 1983; Vandre et al., 1986), by antibodies that recognize activated MEK, ERK, and RSK (Willard and Crouch, 2001), by antibodies that recognize aurora B kinase (Crosio et al., 2002), and by antibodies that recognize citron kinase and its activator RhoA (Madaule et al., 1998). #4381 also stained the midbody area after the robust and widespread mitotic staining disappeared (S.S. and J.K., unpublished data). Therefore, it is possible that some of the mitotic kinases that catalyze S718-S721 phosphorylation remain active at the midbody. Once transformed into open conformation by the activating phosphorylation, the midbody-localized ALIX recruits CHMP4 and interacts with TSG101. These acquired intermolecular interactions of ALIX in turn inhibit reformation of the intramolecular interaction of ALIX even after ALIX dephosphorylation. We have yet to identify the ALIX-activating kinases at the midbody. Although our data indicate that PLK1 is one of the kinases in mitotic cells that catalyzes the activating phosphorylation of ALIX, PLK1 negatively regulates cep55 recruitment to the midbody (Bastos and Barr, 2010), disfavoring this possibility.

EIAV budding neither occurs in M cells nor requires cells to first pass through mitosis. Thus, it is somewhat surprising that S718-S721 phosphorylation is required for ALIX to function in EIAV budding. For this to occur, one potential scenario is that EIAV infection induces the activation of a protein kinase that catalyzes the activating phosphorylation of ALIX. However, when we probed ALIX phosphorylation in EIAV-expressing cells with the phosphospecific antibodies, we did not detect positive signals (S.S. and J.K., unpublished data), suggesting that either EIAV expression did not induce the activating phosphorylation of ALIX, or the induction level was too low to be detected. In any event, it seems improbable that EIAV-expressing cells contain

a level of the activating phosphorylation of ALIX that can independently explain the ALIX activation required for EIAV budding. Another potential scenario is that EIAV-expressing cells contain a low background or induced level of S718-S721 phosphorylation, which cooperates with a viral factor to generate a significant pool of activated ALIX. Since EIAV-expressing cells have high levels of p9 expression, and p9 interaction with phosphorylated ALIX maintains the open conformation of ALIX after ALIX dephosphorylation, it is possible that the combined effects of low levels of ALIX phosphorylation and high levels of p9 expression generate a significant pool of activated ALIX that supports EIAV budding.

EGF-induced downregulation of EGFR is a commonly used model system to study ESCRT-mediated MVB sorting and lysosome targeting of ubiquitinated membrane receptors in vertebrate cells. Our previous studies demonstrated that calcium-dependent ALG-2 interaction with ALIX generates opened ALIX that supports MVB sorting, silencing, and degradation of activated EGFR (Sun et al., 2015a). Since EGF-induced signal transduction activates multiple protein kinases, it is possible that the activating phosphorylation of ALIX cooperates with the ALG-2 dependent mechanism to maximally activate the MVB sorting function of ALIX in EGF-stimulated cells. Results in this study disprove this hypothesis.

MVB sorting of membrane receptors, retroviral budding, and cytokinetic abscission are three classical ESCRT-mediated processes that critically involve ALIX function (Bissig and Gruenberg, 2014; McCullough et al., 2013). Although ALG-2 expression is required for ALIX to function in MVB sorting of activated EGFR, it is not important for ALIX to function in EIAV budding or cytokinetic abscission (Sun et al., 2015a). These results are in sharp contrast to the roles of S718-S721 phosphorylation in the three classical ESCRT-mediated processes. Thus, it seems that the two identified mechanisms of ALIX activation are independently involved in distinct ESCRT-mediated membrane remodeling processes. Since only ALG-2 interaction with ALIX requires calcium, it is possible that ALIX activation by ALG-2 is primarily involved in calcium-dependent ESCRT-mediated processes, whereas the activating phosphorylation of ALIX is primarily involved in calcium-independent ESCRT-mediated processes.

## EXPERIMENTAL PROCEDURES

### Cell Culture, Transfection, and Cell Synchronization

Culture, transfection, and EGF stimulation of HEK293 or HeLa cells were performed as previously described (Sun et al., 2015b). HEK293 cells were synchronized in mitosis through a single thymidine (TdR) (Sigma) block, followed by nocodazole (NC) (Sigma) block (Wu et al., 2014). HEK293 cells were arrested in S phase by a single TdR block. The PLK1 inhibitor BI-2536 (Axon Medchem), PKD inhibitor CID755673 (BioVision), and pan kinase inhibitor staurosporine (LC Laboratories) were dissolved in DMSO and added to culture medium to reach a final concentration of 100 nM, 3 $\mu$M, and 50 nM, respectively. The siRNAs, mammalian expression vectors, and PCR primers used in this study are summarized in Tables S1–S3, respectively.

### Protein Extraction, Immunoblotting, Immunoprecipitation, and Immunostaining

Preparation of crude cell lysates for IB were performed as we previously described (Sun et al., 2015a). Relative signals on immunoblots were quantified by analyzing scanned images with NIH ImageJ version 1.41o. To prepare

cytosolic proteins for IP or GST pull-down, pelleted cells were sonicated with 10 volumes of extraction buffer (EB), consisting of 80 mM β-glycerophosphate, 20 mM EGTA, 15 mM MgCl$_2$, 150 mM NaCl, 1 mM DTT, and proteinase inhibitor cocktail (Sigma) (pH 7.4). For extraction of M cells and occasionally also I cells, EB was freshly supplemented with 1 μM microcystin (Sigma) and 1 mM ATP. Cell lysates were cleared by centrifugation at 16,000 $g$ for 10 min at 4°C. CIP (New England Biolabs) was added to ME/MEE at a final concentration of 1 unit/μg substrate proteins. Samples were immunoprecipitated with the indicated antibodies, and immunocomplexes were washed five times with EB. To prepare cell lysates for dIP, pelleted cells were re-suspended with 10 volumes of denaturing buffer consisting of 50 mM Tris-HCl (pH 7.5), 1% SDS, and 5 mM DTT, and sonicated. After the samples were boiled for 5 min and cleared by centrifugation at 16,000 $g$ for 5 min, they were diluted 10-fold with an SDS-neutralizing IP buffer consisting of 50 mM Tris-HCl (pH 7.5), 250 mM NaCl, 5 mM EDTA, 0.5% NP-40, 1 mM DTT (Tansey, 2007), and proteinase inhibitor cocktail (Sigma). Samples were immunoprecipitated with the indicated antibodies, and immunocomplexes were washed five times with the IP buffer. Production of αpS2 and immunostaining are described in Supplemental Experimental Procedures.

### In Vitro Phosphorylation of ALIX Fragments with *Xenopus* Extracts and GST Pull-Down

MEE and IOE were prepared as previously described (Wu et al., 2010). In vitro transcription and linked translation was performed by using the TNT Quick Coupled Transcription/Translation System (Promega). GST and GST-tagged proteins were produced and purified using our standard procedures (Che et al., 1997). The phosphorylation reaction included one volume of substrate proteins and three volumes of IOE or MEE. The reaction was performed at 22°C for 2 hr unless otherwise indicated, and terminated by adding SDS-PAGE sample buffer. BI-2536, CID755673, and staurosporine were added to MEE at 4°C 15 min prior to the phosphorylation reaction to reach a final concentration of 2 μM, 5 μM, and 5 μM, respectively. GST-tagged proteins were absorbed onto glutathione (GSH) beads (GenScript) at 4°C for 2 hr. After GSH beads were washed five times with EB, proteins remaining on the beads were eluted with SDS-PAGE sample buffer for IB.

### EIAV VLP Release Assay, Membrane Flotation Centrifugation, and Proteinase K Protection Assay

Assays of virus-like particle (VLP) release from HEK293 cells transfected with the pEV53B EIAV$^{Gag}$ vector, fractionation of the PNS of crude lysates of HEK293 cells by membrane flotation centrifugation, and measurement of MVB sorting of activated EGFR by the Proteinase K protection assay were performed exactly as we previously described (Sun et al., 2015b).

### Statistical Analysis
Statistical analyses were performed using Student's $t$ test.

### SUPPLEMENTAL INFORMATION

Supplemental Information includes Supplemental Experimental Procedures, five figures, and four tables and can be found with this article online at http://dx.doi.org/10.1016/j.devcel.2016.01.001.

### AUTHOR CONTRIBUTIONS

S.S. designed and performed most of the experiments and participated in writing the manuscript; L.S. generated αpS2; X.Z. performed some of the pilot experiments; C.W. and R.W. contributed critical reagents and participated in manuscript preparation; S.L. participated in data analyses and writing the manuscript; and J.K. directed the project and wrote the manuscript.

### ACKNOWLEDGMENTS

### REFERENCES

Babst, M., Katzmann, D.J., Estepa-Sabal, E.J., Meerloo, T., and Emr, S.D. (2002a). Escrt-III: an endosome-associated heterooligomeric protein complex required for mvb sorting. Dev. Cell *3*, 271–282.

Babst, M., Katzmann, D.J., Snyder, W.B., Wendland, B., and Emr, S.D. (2002b). Endosome-associated complex, ESCRT-II, recruits transport machinery for protein sorting at the multivesicular body. Dev. Cell *3*, 283–289.

Bastos, R.N., and Barr, F.A. (2010). Plk1 negatively regulates Cep55 recruitment to the midbody to ensure orderly abscission. J. Cell Biol. *191*, 751–760.

Bissig, C., and Gruenberg, J. (2014). ALIX and the multivesicular endosome: ALIX in Wonderland. Trends Cell Biol. *24*, 19–25.

Caillat, C., Macheboeuf, P., Wu, Y., McCarthy, A.A., Boeri-Erba, E., Effantin, G., Gottlinger, H.G., Weissenhorn, W., and Renesto, P. (2015). Asymmetric ring structure of Vps4 required for ESCRT-III disassembly. Nat. Commun. *6*, 8781.

Carlson, L.A., and Hurley, J.H. (2012). In vitro reconstitution of the ordered assembly of the endosomal sorting complex required for transport at membrane-bound HIV-1 Gag clusters. Proc. Natl. Acad. Sci. USA *109*, 16928–16933.

Carlton, J.G., and Martin-Serrano, J. (2007). Parallels between cytokinesis and retroviral budding: a role for the ESCRT machinery. Science *316*, 1908–1912.

Carlton, J.G., Agromayor, M., and Martin-Serrano, J. (2008). Differential requirements for Alix and ESCRT-III in cytokinesis and HIV-1 release. Proc. Natl. Acad. Sci. USA *105*, 10541–10546.

Che, S., Weil, M.M., Nelman-Gonzalez, M., Ashorn, C.L., and Kuang, J. (1997). MPM-2 epitope sequence is not sufficient for recognition and phosphorylation by ME kinase-H. FEBS Lett. *413*, 417–423.

Che, S., El-Hodiri, H.M., Wu, C.F., Nelman-Gonzalez, M., Weil, M.M., Etkin, L.D., Clark, R.B., and Kuang, J. (1999). Identification and cloning of xp95, a putative signal transduction protein in *Xenopus* oocytes. J. Biol. Chem. *274*, 5522–5531.

Crosio, C., Fimia, G.M., Loury, R., Kimura, M., Okano, Y., Zhou, H., Sen, S., Allis, C.D., and Sassone-Corsi, P. (2002). Mitotic phosphorylation of histone H3: spatio-temporal regulation by mammalian Aurora kinases. Mol. Cell Biol. *22*, 874–885.

Daub, H., Olsen, J.V., Bairlein, M., Gnad, F., Oppermann, F.S., Korner, R., Greff, Z., Keri, G., Stemmann, O., and Mann, M. (2008). Kinase-selective enrichment enables quantitative phosphoproteomics of the kinome across the cell cycle. Mol. Cell *31*, 438–448.

Davis, F.M., Tsao, T.Y., Fowler, S.K., and Rao, P.N. (1983). Monoclonal antibodies to mitotic cells. Proc. Natl. Acad. Sci. USA *80*, 2926–2930.

Dejournett, R.E., Kobayashi, R., Pan, S., Wu, C., Etkin, L.D., Clark, R.B., Bogler, O., and Kuang, J. (2007). Phosphorylation of the proline-rich domain of Xp95 modulates Xp95 interaction with partner proteins. Biochem. J. *401*, 521–531.

Dephoure, N., Zhou, C., Villen, J., Beausoleil, S.A., Bakalarski, C.E., Elledge, S.J., and Gygi, S.P. (2008). A quantitative atlas of mitotic phosphorylation. Proc. Natl. Acad. Sci. USA *105*, 10762–10767.

Fisher, R.D., Chung, H.Y., Zhai, Q., Robinson, H., Sundquist, W.I., and Hill, C.P. (2007). Structural and biochemical studies of ALIX/AIP1 and its role in retrovirus budding. Cell *128*, 841–852.

Gershony, O., Pe'er, T., Noach-Hirsh, M., Elia, N., and Tzur, A. (2014). Cytokinetic abscission is an acute G1 event. Cell Cycle *13*, 3436–3441.

Golsteyn, R.M., Mundt, K.E., Fry, A.M., and Nigg, E.A. (1995). Cell cycle regulation of the activity and subcellular localization of Plk1, a human protein kinase implicated in mitotic spindle function. J. Cell Biol. *129*, 1617–1628.

Henne, W.M., Buchkovich, N.J., and Emr, S.D. (2011). The ESCRT pathway. Dev. Cell *21*, 77–91.

Henne, W.M., Stenmark, H., and Emr, S.D. (2013). Molecular mechanisms of the membrane sculpting ESCRT pathway. Cold Spring Harb. Perspect. Biol. *5*, a016766.

Hurley, J.H. (2015). ESCRTs are everywhere. EMBO J. *34*, 2398–2407.

Katzmann, D.J., Babst, M., and Emr, S.D. (2001). Ubiquitin-dependent sorting into the multivesicular body pathway requires the function of a conserved endosomal protein sorting complex, ESCRT-I. Cell *106*, 145–155.

Kienzle, C., Eisler, S.A., Villeneuve, J., Brummer, T., Olayioye, M.A., and Hausser, A. (2013). PKD controls mitotic Golgi complex fragmentation through a Raf-MEK1 pathway. Mol. Biol. Cell *24*, 222–233.

Kim, J., Sitaraman, S., Hierro, A., Beach, B.M., Odorizzi, G., and Hurley, J.H. (2005). Structural basis for endosomal targeting by the Bro1 domain. Dev. Cell *8*, 937–947.

Lee, S., Joshi, A., Nagashima, K., Freed, E.O., and Hurley, J.H. (2007). Structural basis for viral late-domain binding to Alix. Nat. Struct. Mol. Biol. *14*, 194–199.

Madaule, P., Eda, M., Watanabe, N., Fujisawa, K., Matsuoka, T., Bito, H., Ishizaki, T., and Narumiya, S. (1998). Role of citron kinase as a target of the small GTPase Rho in cytokinesis. Nature *394*, 491–494.

McCullough, J., Fisher, R.D., Whitby, F.G., Sundquist, W.I., and Hill, C.P. (2008). ALIX-CHMP4 interactions in the human ESCRT pathway. Proc. Natl. Acad. Sci. USA *105*, 7687–7691.

McCullough, J., Colf, L.A., and Sundquist, W.I. (2013). Membrane fission reactions of the mammalian ESCRT pathway. Annu. Rev. Biochem. *82*, 663–692.

McCullough, J., Clippinger, A.K., Talledge, N., Skowyra, M.L., Saunders, M.G., Naismith, T.V., Colf, L.A., Afonine, P., Arthur, C., Sundquist, W.I., et al. (2015). Structure and membrane remodeling activity of ESCRT-III helical polymers. Science *350*, 1548–1551.

Morita, E., Sandrin, V., Chung, H.Y., Morham, S.G., Gygi, S.P., Rodesch, C.K., and Sundquist, W.I. (2007). Human ESCRT and ALIX proteins interact with proteins of the midbody and function in cytokinesis. EMBO J. *26*, 4215–4227.

Olsen, J.V., Vermeulen, M., Santamaria, A., Kumar, C., Miller, M.L., Jensen, L.J., Gnad, F., Cox, J., Jensen, T.S., Nigg, E.A., et al. (2010). Quantitative phosphoproteomics reveals widespread full phosphorylation site occupancy during mitosis. Sci. Signal. *3*, ra3.

Pashkova, N., Gakhar, L., Winistorfer, S.C., Sunshine, A.B., Rich, M., Dunham, M.J., Yu, L., and Piper, R.C. (2013). The yeast Alix homolog Bro1 functions as a ubiquitin receptor for protein sorting into multivesicular endosomes. Dev. Cell *25*, 520–533.

Schmidt, M.H., Dikic, I., and Bogler, O. (2005). Src phosphorylation of Alix/AIP1 modulates its interaction with binding partners and antagonizes its activities. J. Biol. Chem. *280*, 3414–3425.

Strack, B., Calistri, A., Craig, S., Popova, E., and Gottlinger, H.G. (2003). AIP1/ALIX is a binding partner for HIV-1 p6 and EIAV p9 functioning in virus budding. Cell *114*, 689–699.

Sun, S., Zhou, X., Corvera, J., Gallick, G.E., Lin, S.H., and Kuang, J. (2015a). ALG-2 activates the MVB sorting function of ALIX through relieving its intramolecular interaction. Cell Discov. *1*, 15018.

Sun, S., Zhou, X., Zhang, W., Gallick, G.E., and Kuang, J. (2015b). Unravelling the pivotal role of Alix in MVB sorting and silencing of the activated EGFR. Biochem. J. *466*, 475–487.

Tansey, W.P. (2007). Denaturing protein immunoprecipitation from Mammalian cells. CSH Protoc. *2007*, pdb prot4619.

Teis, D., Saksena, S., and Emr, S.D. (2008). Ordered assembly of the ESCRT-III complex on endosomes is required to sequester cargo during MVB formation. Dev. Cell *15*, 578–589.

Vandre, D.D., Davis, F.M., Rao, P.N., and Borisy, G.G. (1986). Distribution of cytoskeletal proteins sharing a conserved phosphorylated epitope. Eur. J. Cell Biol. *41*, 72–81.

von Schwedler, U.K., Stuchell, M., Muller, B., Ward, D.M., Chung, H.Y., Morita, E., Wang, H.E., Davis, T., He, G.P., Cimbora, D.M., et al. (2003). The protein network of HIV budding. Cell *114*, 701–713.

Willard, F.S., and Crouch, M.F. (2001). MEK, ERK, and p90RSK are present on mitotic tubulin in Swiss 3T3 cells: a role for the MAP kinase pathway in regulating mitotic exit. Cell. Signal. *13*, 653–664.

Wu, C.F., Wang, R., Liang, Q., Liang, J., Li, W., Jung, S.Y., Qin, J., Lin, S.H., and Kuang, J. (2010). Dissecting the M phase-specific phosphorylation of serine-proline or threonine-proline motifs. Mol. Biol. Cell *21*, 1470–1481.

Wu, C.F., Liu, S., Lee, Y.C., Wang, R., Sun, S., Yin, F., Bornmann, W.G., Yu-Lee, L.Y., Gallick, G.E., Zhang, W., et al. (2014). RSK promotes G2/M transition through activating phosphorylation of Cdc25A and Cdc25B. Oncogene *33*, 2385–2394.

Yang, B., Stjepanovic, G., Shen, Q., Martin, A., and Hurley, J.H. (2015). Vps4 disassembles an ESCRT-III filament by global unfolding and processive translocation. Nat. Struct. Mol. Biol. *22*, 492–498.

Zhai, Q., Fisher, R.D., Chung, H.Y., Myszka, D.G., Sundquist, W.I., and Hill, C.P. (2008). Structural and functional studies of ALIX interactions with YPX(n)L late domains of HIV-1 and EIAV. Nat. Struct. Mol. Biol. *15*, 43–49.

Zhou, X., Pan, S., Sun, L., Corvera, J., Lin, S.H., and Kuang, J. (2008). The HIV-1 p6/EIAV p9 docking site in Alix is autoinhibited as revealed by a conformation-sensitive anti-Alix monoclonal antibody. Biochem. J. *414*, 215–220.

Zhou, X., Pan, S., Sun, L., Corvera, J., Lee, Y.C., Lin, S.H., and Kuang, J. (2009). The CHMP4b and Src docking sites in the Bro1 domain are autoinhibited in the native state of Alix. Biochem. J. *418*, 277–284.

Zhou, X., Si, J., Corvera, J., Gallick, G.E., and Kuang, J. (2010). Decoding the intrinsic mechanism that prohibits ALIX interaction with ESCRT and viral proteins. Biochem. J. *432*, 525–534.

# Supplemental Information

## Phosphorylation-Dependent Activation

## of the ESCRT Function of ALIX

## in Cytokinetic Abscission and Retroviral Budding

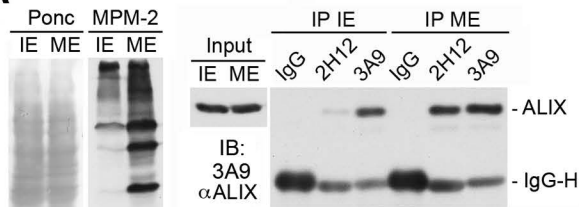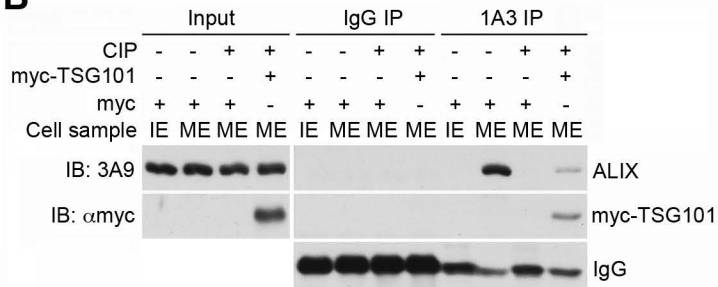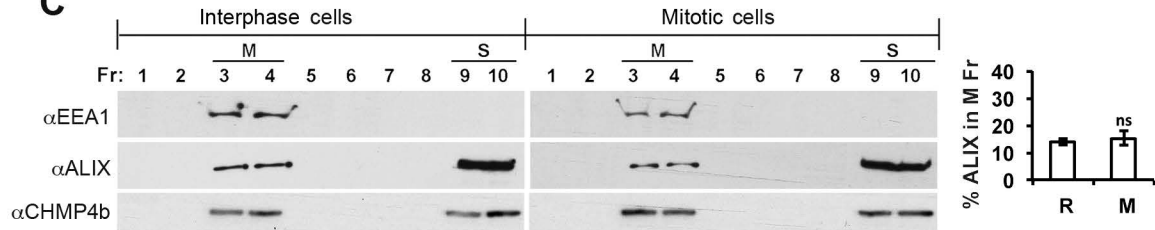**Sheng Sun, Le Sun, Xi Zhou, Chuanfen Wu, Ruoning Wang, Sue-Hwa Lin, and Jian Kuang**

**Figure S1. Supplemental data related to Figure 1.** (A) IE and ME were prepared with EB freshly supplemented with 1 µM microcystin and 1 mM ATP, and immunoprecipitated with indicated anti-ALIX antibodies. Input proteins and immunocomplexes were immunoblotted with indicated antibodies. (B) ME was first incubated with the TNT product of myc or myc-TSG101 at 4ºC for 2 h, and then treated with CIP. IE, ME and the two samples of differently treated ME were immunoprecipitated with indicated antibodies, followed by immunoblotting with indicated antibodies. (C) PNSs from asynchronously growing HEK293 cells (Interphase cells) or mitotically arrested HEK293 cells (Mitotic cells) were fractionated by membrane flotation centrifugation. Same volumes of aliquots were taken and immunoblotted with indicated antibodies; membrane (M) and soluble (S) protein fractions are indicated. The average percentages of ALIX in the M fraction and SDs were determined from three independent experiments and plotted.
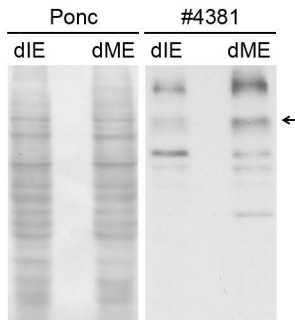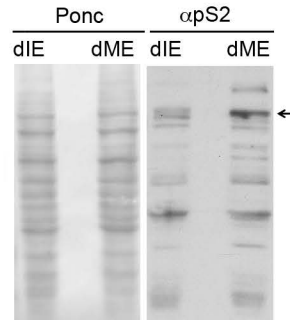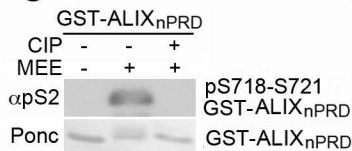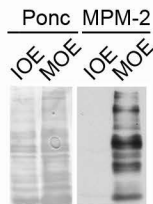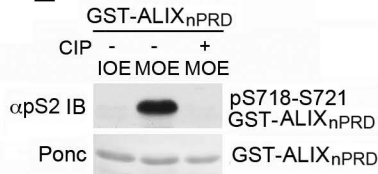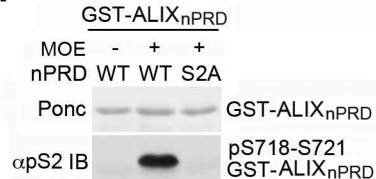
**Figure S2. Supplemental data related to Figure 3.** (A) Left: The phosphospecific sequence recognized by the #4381 antibody, and its alignment with the S718 surrounding sequence in ALIX. Right: SDS-denatured IE and ME (dIE and dME) were immunoblotted with the #4381 antibody after Ponc staining, and the arrow indicates the position of ALIX. (B) Left: Sequence of the phosphorylated ALIX peptide used for production of the anti-pS2 antibody. Right: The dIE and dME were immunoblotted with the anti-pS2 antibody after Ponc staining, and the arrow indicates the position of ALIX. (C) GST-ALIX$_{nPRD}$ was mock-treated or phosphorylated with MEE or MEE plus CIP, and then immobilized onto GSH beads. Bound proteins were immunoblotted with the anti-pS2 antibody. (D) Immature oocytes and progesterone-matured oocytes were extracted with EB supplemented with ATP, and freshly prepared immature oocyte extracts (IOE) and mature oocyte extracts (MOE) were immunoblotted with MPM2. (E) GST-ALIX$_{nPRD}$ was phosphorylated with freshly prepared IOE, MOE, or MOE plus CIP, and then immobilized onto GSH beads. Bound proteins were immunoblotted with the anti-pS2 antibody. (F) WT and S2A GST-ALIX$_{nPRD}$ were mock treated or phosphorylated with MOE, and then immobilized onto GSH beads. Bound proteins were immunoblotted with the anti-pS2 antibody.
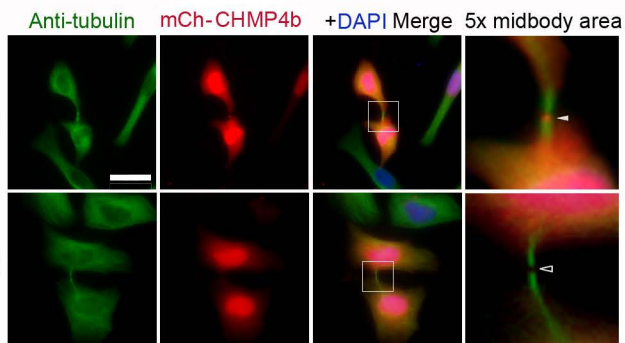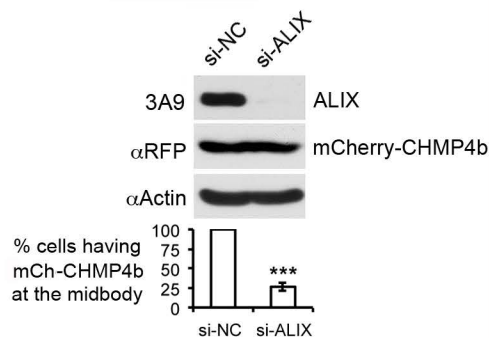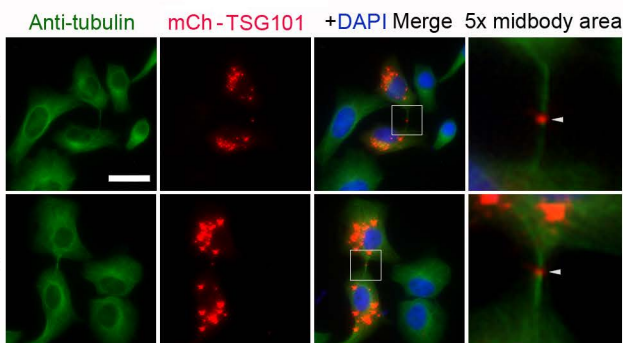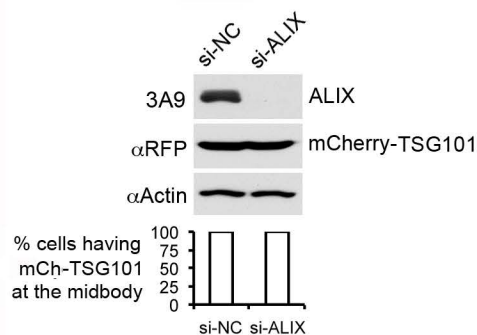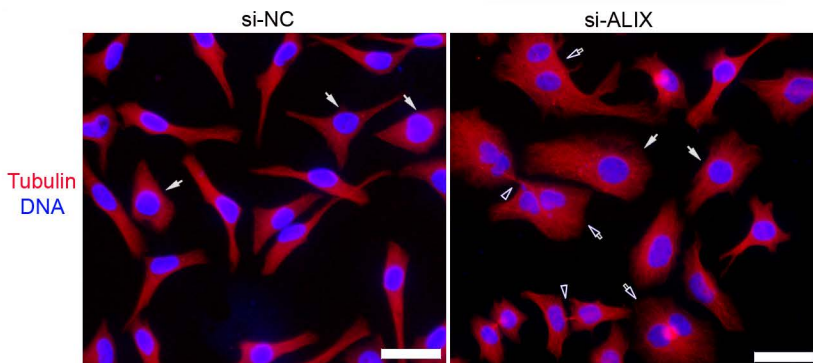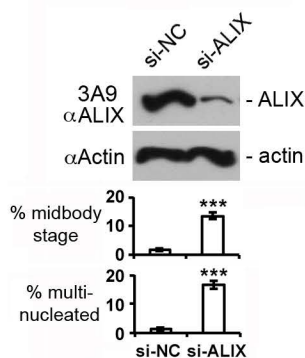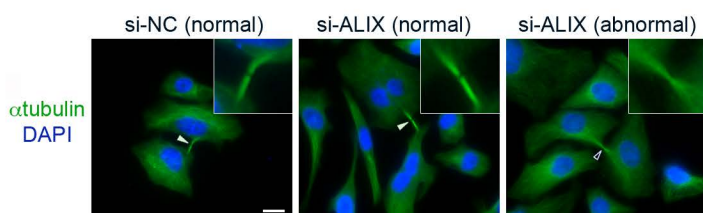
**Figure S3. Supplemental data related to Figure 5.** (A&B) HeLa cells were transfected with indicated agents and cultured as done for Fig. 5A. Cell lysates were immunoblotted with indicated antibodies to visualize ALIX, mCherry-CHMP4b (A), mCherry-TSG101 (B) and actin. Fixed cells were immunostained with anti-tubulin antibody (green), and counterstained with DAPI (blue). The average percentages of mCherry positive cells with midbody localization of mCherry-CHMP4b and SDs (A) or mCherry-TSG101 (B) were determined from three independent experiments and plotted. Representative images are shown; the squares show the midbody areas to be enlarged. Solid and hollow arrowheads indicate the presence and absence of mCherry-CHMP4b (A) or mCherry-TSG101 (B) at the midbody, respectively. Scale bar: 50 μm. (C) HeLa cells were transfected with indicated siRNAs for 72 h, and cell lysates were immunoblotted with indicated antibodies to visualize ALIX and actin. Fixed cells were immunostained with an anti-tubulin antibody (red), and counterstained with DAPI (blue). The average percentages of midbody-stage cells or multinucleated cells and SDs were determined from three independent experiments and plotted. Representative images are shown; solid and hollow arrows indicate mononucleated and multinucleated cells, respectively, and hollow arrowheads indicate midbodies between daughter cells. Scale bar: 50 μm. (D) HeLa cells were transfected with indicated siRNAs for 72 h, and fixed cells were immunostained with an anti-tubulin antibody (green), and counterstained with DAPI (blue). Representative images are shown in which solid and hollow arrowheads indicate midbodies with normal and abnormal morphology, respectively. The squares on the right corner show the 3x enlarged midbody area. The percentages of abnormal midbodies were determined from at least 50 midbody-stage cells. Scale bar: 15 μm.

**Figure S4. Supplemental data related to Figure 6.** IE from HEK293 cells ectopically expressing GFP-ALIX was processed as diagrammed (left panel). Input proteins (middle panel) and immunocomplexes (right panel) were immunoblotted with indicated antibodies to visualize GFP-ALIX, GST, GST-p9 and IgG-H.
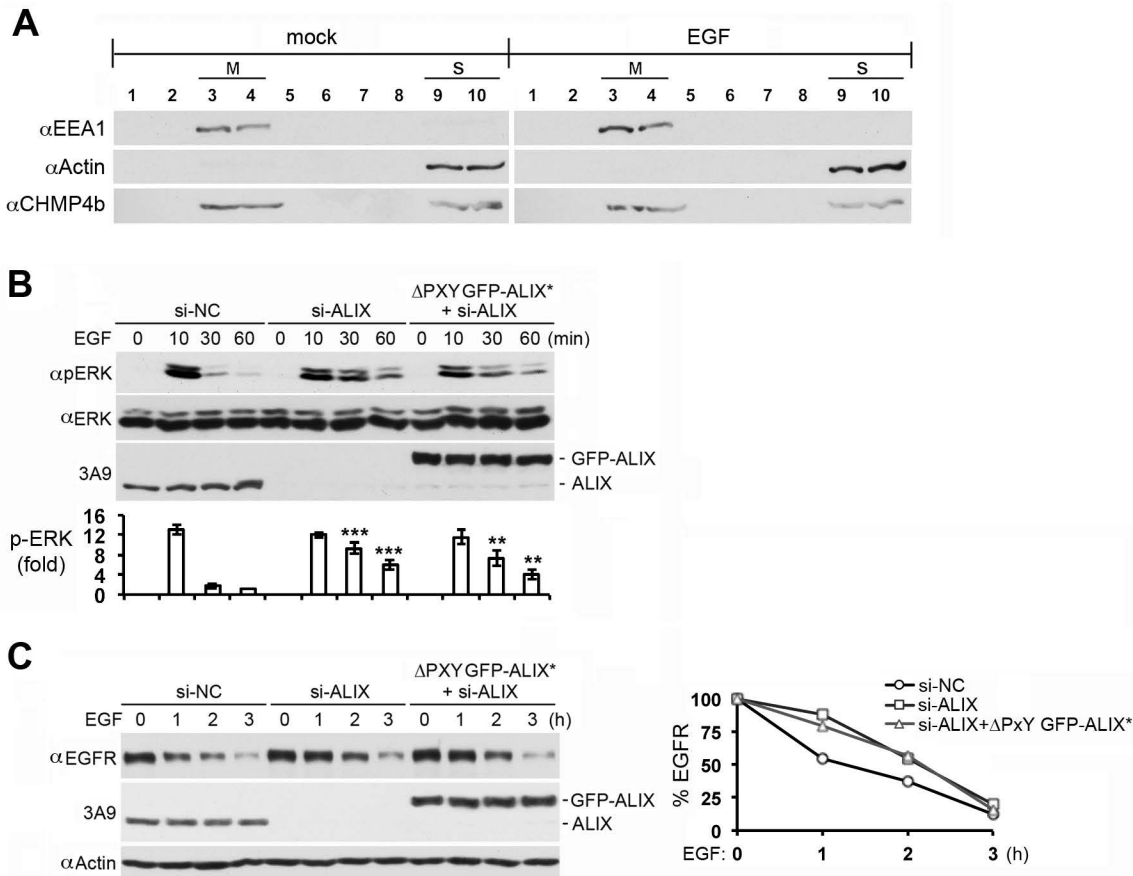
**Figure S5. Supplemental data related to Figure 7.** (A) HEK293 cells ectopically expressing indicated forms of GFP-ALIX were processed as described for Fig. 7A. Same volumes of aliquots were taken and immunoblotted with indicated antibodies. (B) HEK293 cells transfected with indicated siRNAs and the plasmid for ΔPxY GFP-ALIX* were processed as described for Fig. 7 C&D. (C) HEK293 cells transfected with indicated siRNAs and the plasmid for ΔPxY GFP-ALIX* were processed as described as Fig. 7 E&F.

**Table S1. Sequences of siRNAs used in this study - related to Experimental Procedures**

| Target | Name | Sequence | Source |
|---|---|---|---|
| ALIX | si-ALIX | 5'-GAGAAGAAAUUGCAAGGUUdTdT-3' | Sigma-Genosys |
| Firefly GL3 luciferase | si-NC | 5'-CUUACGCUGAGUACUUCGAdTdT-3' | Sigma-Genosys |

**Table S2. Mammalian and bacterial expression vectors used in this study – related to Experimental Procedures**

| Vector | Source | Reference |
|---|---|---|
| 1. pEGFP-C3-based mammalian expression vector for GFP-ALIX | A gift from Dr. Masatoshi Maki (Nagoya, Japan) | (Shibata et al., 2004) |
| 1a. pEGFP-C3-based mammalian expression vector for ALIX-siRNA-insensitive GFP-ALIX (GFP-ALIX*) | Site-directed mutagenesis of vector 1 | new |
| 1b. pEGFP-C3-based mammalian expression vector for S718A GFP-ALIX | Site-directed mutagenesis of vector 1 | new |
| 1c. pEGFP-C3-based mammalian expression vector for S721A GFP-ALIX | Site-directed mutagenesis of vector 1 | new |
| 1d. pEGFP-C3-based mammalian expression vector for S718A-S721A GFP-ALIX | Site-directed mutagenesis of vector 1 | new |
| 1e. pEGFP-C3-based mammalian expression vector for S712A-S729A GFP-ALIX | Site-directed mutagenesis of vector 1 | new |
| 1f. pEGFP-C3-based mammalian expression vector for S718A-S721A ALIX-siRNA-insensitive GFP-ALIX (S2A GFP-ALIX*) | Site-directed mutagenesis of vector 1a | new |
| 1g. pEGFP-C3-based mammalian expression vector for S712A-S729A ALIX-siRNA-insensitive GFP-ALIX (S2A- GFP-ALIX*) | Site-directed mutagenesis of vector 1e | new |
| 1h. pEGFP-C3-based mammalian expression vector for S718D-S721D GFP-ALIX | Site-directed mutagenesis of vector 1 | new |
| 2. pCMV-based mammalian expression vector for FLAG-CHMP4b | A gift from Dr. Masatoshi Maki (Nagoya, Japan) | (Katoh et al., 2003) |
| 3. pIRES2 based mammalian expression vector for FLAG–TSG101 | A gift from Dr. Wesley I. Sundquist (Salt Lake City, UT) | (von Schwedler et al., 2003) |
| 4. pmCherry-C1-based expression vector for mCherry-CHMP4b | Cut the CHMP4b fragment in vector 2 by EcoRI and XhoI and insert it into the pmCherry-C1 vector (Clontech) after digestion with EcoRI and SalI. | new |
| 5. pmCherry-C1-based expression vector for mCherry-TSG101 | PCR amplification of coding region of TSG101 from pIRES2-FLAG–TSG101, followed by subcloning into pmCherry-C1 vector (clontech). | new |
| 6. pEV53B-based mammalian expression vector for infection defective EIAV | A gift from Dr. John Olsen (Chapel Hill, NC) | (Olsen, 1998) |
| 7. pCS2-MT based TNT expression vector for myc-ALIX$_{nPRD}$ | PCR amplification of coding region of amino acid 706-786 of WT GFP-ALIX, followed by subcloning into pCS2-MT vector (clontech) | new |
| 8. pCS2-MT based TNT expression vector for S718A-S721A myc-ALIX$_{nPRD}$ | PCR amplification of coding region of amino acid 706-786 of S718A-S721A GFP-ALIX, followed by subcloning into pCS2-MT vector (clontech) | new |
| 9. pCS2-MT based TNT expression vector for S712A-S729A myc-ALIX$_{nPRD}$ | PCR amplification of coding region of amino acid 706-786 of S712A-S729A GFP-ALIX, followed by subcloning into pCS2-MT vector (clontech) | new |
| 10. pCS2-MT based TNT expression vector for S718D-S721D myc-ALIX$_{nPRD}$ | PCR amplification of coding region of amino acid 706-786 of S718D-S721D GFP-ALIX, followed by subcloning into pCS2-MT vector (clontech) | new |
| 11. pCS2-MT based TNT expression vector for myc-TSG101 | PCR amplification of coding region of TSG101 from pIRES2-FLAG–TSG101, followed by subcloning into pCS2-MT vector (clontech) | new |

| | | |
|---|---|---|
| 12. pCS2-HA based expression vector for HA-Plx1 (Xenopus) | PCR amplification of coding region of Plx1 from pBluescript-Plx1(A gift from Dr. William G. Dunphy (Kumagai and Dunphy, 1996), followed by subcloning into pCS2-HA vector (clontech) | new |
| 13. pCS2-HA based expression vector for HA-K82R Plx1 (Xenopus) | PCR amplification of coding region of K82R Plx1 from pBluescript-K82R Plx1, followed by subcloning into pCS2-HA vector (clontech) | new |
| 14. pGEX-4T3 based bacterial expression vector GST-ALIX$_{nPRD}$ | PCR amplification of coding region of amino acid 706-786 of WT GFP-ALIX, followed by subcloning into pGEX-4T3 vector (Amersham Biosciences) | new |
| 15. pGEX-4T3 based bacterial expression vector for GST-ALIX$_{Bro1}$ | Generated in our previous studies | (Pan et al., 2006) |
| 16. pGEX-4T3 based bacterial expression vector for GST-ALIX$_{1-746}$ | Generated in our previous studies | (Zhou et al., 2010) |
| 17. pGEX-4T3 based bacterial expression vector for GST-CHMP4b | PCR amplification of coding region of CHMP4b from FLAG-CHMP4b, followed by subcloning into pGEX-4T3 vector (Amersham Biosciences) | new |
| 18. pGEX-4T3 based bacterial expression vector for GST-p9$^{Gag}$ | A gift from Dr. Wesley I. Sundquist (Salt Lake City, UT) | (Fisher et al., 2007) |

**Table S3. PCR primers used for site-directed mutagenesis and making vectors – related to Experimental Procedures**

| Product | Primers (Forward/Reverse) | Template |
|---|---|---|
| 1a. ALIX-siRNA-insensitive GFP-ALIX | 5'-GAAGAAATTTGGGGAGGAGATCGCGAGATTACAGCATGCAGCAG-3'<br>5'-CTGCTGCATGCTGTAATCTCGCGATCTCCTCCCCAAATTTCTTC-3' | 1. WT GFP-ALIX |
| 1b. S718A GFP-ALIX | 5'-CATTGCCAGAGAACCTGCTGCTCCTTCAATTCCTACAC-3'<br>5'-GTGTAGGAATTGAAGGAGCAGCAGGTTCTCTGGCAATG-3' | 1. WT GFP-ALIX |
| 1c. S721A GFP-ALIX | 5'-GAACCTAGTGCTCCTGCAATTCCTACACCTGC-3'<br>5'-GCAGGTGTAGGAATTGCAGGAGCACTAGGTTC-3' | 1. WT GFP-ALIX |
| 1d. S718A-S721A GFP-ALIX | 5'-CATTGCCAGAGAACCTGCTGCTCCTGCAATTCCTACACCTG-3'<br>5'-CAGGTGTAGGAATTGCAGGAGCAGCAGGTTCTCTGGCAATG-3' | 1. WT GFP-ALIX |
| 1e. S712A-S729A GFP-ALIX | WT to S712A:<br>5'-CTTAAAGGACTTGCAACAAGCCATTGCCAGAGAACCTAGTG-3'<br>5'-CACTAGGTTCTCTGGCAATGGCTTGTTGCAAGTCCTTTAAG -3'<br>S712A to S712A/S729A:<br>5'-CTACACCTGCGTATCAGGCCTCACCAGCAGGAGGAC-3'<br>5'-GTCCTCCTGCTGGTGAGGCCTGATACGCAGGTGTAG-3' | 1. WT GFP-ALIX |
| 1f. S718A-S721A ALIX-siRNA-insensitive GFP-ALIX | 5'-CATTGCCAGAGAACCTGCTGCTCCTGCAATTCCTACACCTG-3'<br>5'-CAGGTGTAGGAATTGCAGGAGCAGCAGGTTCTCTGGCAATG-3' | 1a. ALIX-siRNA-insensitive GFP-ALIX |
| 1g. S712A-S729A ALIX-siRNA-insensitive GFP-ALIX | 5'-GAAGAAATTTGGGGAGGAGATCGCGAGATTACAGCATGCAGCAG-3'<br>5'-CTGCTGCATGCTGTAATCTCGCGATCTCCTCCCCAAATTTCTTC-3' | 1e. S712A-S729A GFP-ALIX |
| 1h. S718D-S721D GFP-ALIX | 5'-GCATTGCCAGAGAACCTGATGCTCCTGATATTCCTACACCTGCG-3'<br>5'-CGCAGGTGTAGGAATATCAGGAGCATCAGGTTCTCTGGCAATGC-3' | 1. WT GFP-ALIX |
| 5. mCherry-TSG101 | 5'-TAACTCGAGCT ATGGCGGTGTCGGAGAG-3' (Xho I)<br>5'- TAAGAATTCTCAGTAGAGGTCACTGAGACCG-3' (EcoRI) | 3. pIRES2-FLAG-TSG101 |
| 7. pCS2-MT-ALIX$_{nPRD}$ | 5'-TAAGAATTCATTAAAGGACTTGCAACAAGCATTG-3' (EcoRI)<br>5'-TAACTCGAGTGGCGCAGCAGTCCC-3' (Xho I) | 1. WT GFP-ALIX |
| 8. pCS2-MT-S718A-S721A ALIX$_{nPRD}$ | 5'-TAAGAATTCATTAAAGGACTTGCAACAAGCATTG-3' (EcoRI)<br>5'-TAACTCGAGTGGCGCAGCAGTCCC-3' (Xho I) | 1d. S718A-S721A GFP-ALIX |
| 9. pCS2-MT-S712A-S729A ALIX$_{nPRD}$ | 5'-TAAGAATTCATTAAAGGACTTGCAACAAGCCATTG-3' (EcoRI)<br>5'-TAACTCGAGTGGCGCAGCAGTCCC-3' (Xho I) | 1e. S712A-S729A GFP-ALIX |
| 10. pCS2-MT-S718D-S721D myc-ALIX$_{nPRD}$ | 5'-TAAGAATTCATTAAAGGACTTGCAACAAGCATTG-3' (EcoRI)<br>5'-TAACTCGAGTGGCGCAGCAGTCCC-3' (Xho I) | 1h. S718D-S721D GFP-ALIX |
| 11. pCS2-MT-TSG101 | 5'- TAAGAATTCAATGGCGGTGTCGGAGAG-3' (EcoRI)<br>5'- TAACTCGAGTCAGTAGAGGTCACTGAGACCG-3' (Xho I) | 3. pIRES2-FLAG-TSG101 |
| 12. pCS2-HA-Plx1 (*Xenopus*) | 5'-AATGGGCCCTCAAGTGGCCGGTAAGAAAC-3' (Apa I)<br>5'-GCCTCTAGAGCCGAGGCCTTTACGTGTGC-3' (Xba I) | pBluescript-Plx1 |
| 13. pCS2-HA-Plx1 K82R (*Xenopus*) | 5'-AATGGGCCCTCAAGTGGCCGGTAAGAAAC-3' (Apa I)<br>5'-GCCTCTAGAGCCGAGGCCTTTACGTGTGC-3' (Xba I) | pBluescript-Plx1 K82R |
| 14. pGEX-4T3-ALIX$_{nPRD}$ | 5'-TAAGAATTCCTTAAAGGACTTGCAACAAGCATTG-3' (EcoRI)<br>5'-TAACTCGAGTGGCGCAGCAGTCCC-3' (Xho I) | 1. WT GFP-ALIX |
| 17. pGEX-4T3-CHMP4b | 5'- TAAGAATTCCATGTCGGTGTTCGGGAAG-3' (EcoRI)<br>5'- TAACTCGAGTTACATGGATCCAGCCCAG-3' (Xho I) | 2. FLAG-CHMP4b |

**Table S4. Antibodies used in this study – related to Experimental Procedures**

| Antibody | Recognition | Type | Source | Use |
|---|---|---|---|---|
| 1A3 anti-ALIX | ALIX (Y319)/ Xp95(Y318) | Mouse monoclonal | Made in our previous studies | Immunoblotting Immunoprecipitation |
| 1A12 anti-ALIX | ALIX$_{605-709}$ | Mouse monoclonal | Made in our previous studies | Immunoprecipitation |
| 2H12 anti-ALIX | ALIX$_{F676\ pocket}$ | Mouse monoclonal | Made in our previous studies | Immunoprecipitation |
| 3A9 anti-ALIX | ALIX$_{605-709}$ | Mouse monoclonal | Made in our previous studies | Immunoblotting Immunoprecipitation |
| anti-actin | Actin | Mouse monoclonal | Sigma-Aldrich Cat#: A5441 | Immunoblotting |
| anti-tubulin | Alpha-tubulin | Rabbit monoclonal | Cell Signaling Cat#: 2125S | Immunostaining |
| anti-CA | EIAV capsid antigen (CA) | Mouse monoclonal | A gift from Dr. Robert Mealey (Pullman, WA) | Immunoblotting |
| anti-CHMP4b | CHMP4b | Rabbit polyclonal | Santa Cruz Cat#: sc-134946 | Immunoblotting |
| anti-EEA1 | EEA1 | Rabbit monoclonal | Epitomics Cat#: 3704-1 | Immunoblotting |
| anti-EGFR | EGFR | Rabbit monoclonal | Epitomics Cat#: 1902-1 | Immunoblotting |
| anti-ERK1 | ERK1 | Rabbit polyclonal | Santa Cruz Cat#:sc-94 | Immunoblotting |
| anti-ERK2 | ERK2 | Rabbit polyclonal | Santa Cruz Cat#:sc-154 | Immunoblotting |
| anti-FLAG | FLAG epitope | Mouse monoclonal | Pierce Cat#: MA1-918781 | Immunoblotting |
| anti-FLAG | FLAG epitope | Rabbit polyclonal | Santa Cruz Cat#: sc-807 | Immunoblotting Immunoprecipitation |
| anti-GFP | GFP | Mouse monoclonal | Santa Cruz Cat#: sc-9996 | Immunoblotting Immunoprecipitation Immunostaining |
| anti-GST | GST | Rabbit polyclonal | Santa Cruz Cat#: sc-459 | Immunoblotting |
| anti-HA | HA epitope | Rabbit polyclonal | Santa Cruz Cat#: sc-805 | Immunoblotting Immunoprecipitation |
| IgG | IgG | Mouse | Sigma-Aldrich Cat#: I5381-10MG | Immunoprecipitation |
| IgG | IgG | Rabbit | Sigma-Aldrich Cat#: I5006-10MG | Immunoprecipitation |
| anti-myc | myc epitope | Rabbit polyclonal | Santa Cruz Cat#: sc-789 | Immunoblotting Immunoprecipitation |
| MPM2 | Mitotic phosphoproteins | Mouse monoclonal | Lab reserve | Immunoblotting |
| #4381 antibody | PKD substrates | Rabbit polyclonal | Cell Signaling Cat#: 4381 | Immunoblotting Immunoprecipitation |
| anti-pS2 antibody | p-S718-S721-ALIX | Rabbit polyclonal | Made in this study | Immunoblotting Immunoprecipitation |
| anti-p-ERK | p-ERK1/2 at Tyr 204 | Mouse monoclonal | Santa Cruz Cat#: sc7383 | Immunoblotting |
| anti-RFP | mCherry epitope | Mouse monoclonal | Pierce Cat#: MA5-15257 | Immunoblotting |
| anti-p-Tyr | phosphotyrosine | Mouse monoclonal | Cell Signaling Cat#: 9416 | Immunoblotting |
| anti-TSG101 | TSG101 | Rabbit monoclonal | Epitomics Cat#: 5377-1 | Immunoblotting |

**SUPPLEMENTAL EXPERIMENTAL PROCEDURES**

**In vitro phosphorylation of ALIX fragments with *Xenopus* extracts and GST pull-down**

In vitro transcription and linked translation of proteins was performed by using TNT® Quick Coupled Transcription/Translation System (Promega) according to the manufacturers' instructions. GST and GST-tagged proteins were produced and purified using our standard procedures (Che et al., 1997). Phosphorylation reaction included one volume of substrate proteins and three volumes of IOE or MEE. The reaction was performed at 22ºC for 2 h unless otherwise indicated, and terminated by adding SDS-PAGE sample buffer. The Plk1 inhibitor BI-2536 (Axon Medchem), the PKD inhibitor CID755673 (BioVision Inc.), and the pan-kinase inhibitor staurosporine (LC Laboratories) were all dissolved in Dimethyl sulfoxide (DMSO), and added to MEE at 4ºC whenever indicated 15 min prior to the phosphorylation reaction to reach a final concentration of 2 µM, 5 µM and 5 µM, respectively. GST tagged proteins were immobilized onto glutathione (GSH) beads (GenScript), and GST pull-down was performed at 4°C for 2 h. After GSH beads were washed five times with EB, proteins remaining on the beads were eluted with SDS-PAGE sample buffer for immunoblotting.

**Immunostaining and fluorescence microscopy**

Transfected HeLa cells were subcultured into chamber slides (Nunc Lab-Tek) coated with poly-D-Lysine (Cultrex) and cultured for 48 h before being fixed with 4% (w/v) of Paraformaldehyde at room temperature for 20 min. Fixed cells were permeabilized with 0.2% Triton X-100 in PBS followed by blocking with 1x blocking buffer (1% BSA, 0.25% horse serum, 0.2% Triton X-100 in PBS). Blocked cells were first stained with primary antibodies in 0.1x blocking buffer at 4ºC overnight, and then with Alexa Fluor 568, Alexa Fluor 488 or Alexa Fluor 647 conjugated secondary antibodies in TBST (0.1% Triton X-100 in TBS) at room temperature for 1 h. Nuclei were stained with DAPI (Sigma). Images were acquired using MetaMorph software (7.7.5.0) on ZEISS Axioplan2 image system (Objective: plan-NEOFLUAR 20×/0.50). For obtaining the percentages of the midbody localization of mCherry-CHMP4b or mCherry-TSG101 in midbody-staged cells with knockdown of ALIX, at least 10 clearly mCherry positive cells were counted for each experiment. For obtaining the percentages of the midbody localization of mCherry-CHMP4b in midbody-staged cells ectopically expressing both GFP-ALIX* and mCherry-CHMP4b, at least 10 clearly double positive cells were counted for each experiment. For obtaining the percentages of multinucleated or midbody-staged cells induced by ALIX knockdown, at least 200 cells were counted for each experiment. For obtaining the percentages of multinucleated or midbody-staged cells ectopically expressing GFP or GFP-ALIX*, at least 100 clearly GFP-positive cells were counted for each experiment. There are four types of GFP-ALIX transfected cells under our fluorescence microscope. (i) No over-background green signal. (ii) Low over-background green signal without clear cell contour. (iii) Easily discernible over-background green signal with clear cell contour and specific localization in the cytoplasm. (iv) Very bright green cells with rounded cell shape, suggesting cell toxicity. We specifically examined the third type of cells.

**Generation of rabbit polyclonal antibodies recognizing phosphorylated Ser718 and Ser721 at ALIX**

To prepare antigen, a synthetic phosphopeptide consisting of the residues 711 to 724 of ALIX and phosphorylated at both Ser718 and Ser721 (CSIAREP(pS)AP(pS)IPT) was conjugated to keyhole limpet hemocyanin (KLH). To generate rabbit polyclonal antibodies, rabbits were immunized with the conjugated phosphopeptide for 42 days, and immunesera were collected. The IgG fraction of the antibodies was purified by protein G affinity chromatography. The phosphospecificity of the purified antibodies were evaluated with the enzyme-linked immune sorbent assay (ELISA).

## SUPPLEMENTAL REFERENCES

Che, S., Weil, M.M., Nelman-Gonzalez, M., Ashorn, C.L., and Kuang, J. (1997). MPM-2 epitope sequence is not sufficient for recognition and phosphorylation by ME kinase-H. FEBS Letter *413*, 417-423.

Fisher, R.D., Chung, H.Y., Zhai, Q., Robinson, H., Sundquist, W.I., and Hill, C.P. (2007). Structural and biochemical studies of ALIX/AIP1 and its role in retrovirus budding. Cell *128*, 841-852.

Katoh, K., Shibata, H., Suzuki, H., Nara, A., Ishidoh, K., Kominami, E., Yoshimori, T., and Maki, M. (2003). The ALG-2-interacting protein Alix associates with CHMP4b, a human homologue of yeast Snf7 that is involved in multivesicular body sorting. J Biol Chem *278*, 39104-39113. Epub 32003 Jul 39114.

Kumagai, A., and Dunphy, W.G. (1996). Purification and molecular cloning of Plx1, a Cdc25-regulatory kinase from Xenopus egg extracts. Science *273*, 1377-1380.

Olsen, J.C. (1998). Gene transfer vectors derived from equine infectious anemia virus. Gene Ther *5*, 1481-1487.

Pan, S., Wang, R., Zhou, X., He, G., Koomen, J., Kobayashi, R., Sun, L., Corvera, J., Gallick, G.E., and Kuang, J. (2006). Involvement of the adaptor protein Alix in actin cytoskeleton assembly. J Biol Chem *285*, 34640-34650.

Shibata, H., Yamada, K., Mizuno, T., Yorikawa, C., Takahashi, H., Satoh, H., Kitaura, Y., and Maki, M. (2004). The penta-EF-hand protein ALG-2 interacts with a region containing PxY repeats in Alix/AIP1, which is required for the subcellular punctate distribution of the amino-terminal truncation form of Alix/AIP1. J Biochem (Tokyo) *135*, 117-128.

von Schwedler, U.K., Stuchell, M., Muller, B., Ward, D.M., Chung, H.Y., Morita, E., Wang, H.E., Davis, T., He, G.P., Cimbora, D.M.*, et al.* (2003). The protein network of HIV budding. Cell *114*, 701-713.

Zhou, X., Si, J., Corvera, J., Gallick, G.E., and Kuang, J. (2010). Decoding the intrinsic mechanism that prohibits ALIX interaction with ESCRT and viral proteins. Biochem J *432*, 525-534.